SUPPORTING INFORMATION

Stabilization of cyclin dependent kinase 4 by methionyl-tRNA synthetase in p16^{INK4a}-negative cancer

Nam Hoon Kwon, Jin Young Lee, Ye-lim Ryu, Chanhee Kim, Jiwon Kong, Seongeun Oh, Beom Sik Kang, Hye Won Ahn, Sung Gwe Ahn, Joon Jeong, Hoi Kyoung Kim, Jong Hyun Kim, Dae Young Han, Min Chul Park, Doyeun Kim, Ryuichi Takase, Isao Masuda, Ya-Ming Hou, Sung Ill Jang, Yoon Soo Chang, Dong Ki Lee, Youngeun Kim, Ming-Wei Wang, Basappa, and Sunghoon Kim

Materials and Methods

BiFC assay and immunofluorescence imaging. MRS was cloned into p-BiFC-VC155 with an HA tag, and WRS and CDK4 were cloned into p-BiFC-VN173 with a Flag tag. H460 cells were seeded on a cover slip and co-transfected with the pBiFC-VC155-MRS and pBiFC-VN173-WRS or pBiFC-VN173-CDK4 for 24 h. The cells were treated with 50 μM MG132 for 2 h before 50 μM FSMO treatment and then further incubated for 6 h in the presence of 50 μM MG132, 50 μM FSMO, and 2% FBS. After fixing with pre-chilled 100% methanol for 7 min and blocking with 3% CAS for 15 min at RT, cells were incubated with Flag or HA antibodies for 1 h overnight and treated with Alexa Fluor 594- and Alexa Fluor 647-conjugated secondary antibodies for 1 h. The nuclei were stained with DAPI solution for 10 min in the dark. The fluorescence was examined by confocal microscopy at 60 × magnification.

NanoBiT assay. CHO-K1 cells were transfected with 0.5 μg each of pBiT1.1-C [TK/LgBiT] vector cloned with CDK4 and pBiT2.1-C [TK/SmBiT] vector with inserted HSP90 and with different concentrations of pEXPR-IBA105-MRS plasmid (from 0.13 to 2 μg). After 48 h of incubation, cells were incubated with Nano-Glo live cell substrate (Promega) and buffer (Promega), and the luminescence was read with a Glomax 96

microplate luminometer (Promega).

MARS genetrap mice and *in vivo* translation monitoring. *MARS* genetrap mice were derived from MarsGt(AT0330) Wtsi embryonic stem (ES) cells (Lexicon Genetics), where the pGT0lxr vector was inserted in intron 19 of the *MARS* gene. Using the ES cells, *MARS* knockout mice were generated at the University of California, Davis, Mouse Biology Program. Genotyping primers were designed flanking the genetrap insertion site (Mars common forward, 5'-CGATGGTGCTGGGTACACTTC-3'; Mars WT reverse, 5'-GAAAATGAGATGGATTGGCAGATGTAG-3'; Mars Mut reverse, 5'-AGGTCACACGCACATCCCAAAG-3'). Homozygotes were viable and produced according to the Mendelian ratio. Mice were backcrossed and maintained in the C57Bl/6J background. For *in vivo* aminoacylation monitoring, 6-week-old female MRS WT and homozygous mice were directly injected with 1 mCi (100 μL) of [^{35}S]Met (1,000 Ci/mmol; PerkinElmer) via the tail vein. After 4 h, the mice were sacrificed, and the brain, kidney, thymus, spleen, lung, liver, pancreas, intestine, colon, and heart were excised. Each organ was grounded using a mortar and pestle. A total of 30 μg protein was separated by SDS-PAGE and detected by autoradiography. Two female siblings without radioisotope injection were also sacrificed, and each organ was collected and processed for the immunoblot analysis. Animal experiments complied with the University Animal Care and Use Committee guidelines at Seoul National University.

***In vitro* pull-down assay.** GST-fusion proteins were expressed in *Escherichia coli* (*E. coli*) Rosetta2 and induced with 1 mM IPTG for 16 h at 37 °C. Harvested cells were lysed by sonication, and lysates were incubated with glutathione Sepharose 4B (GE Healthcare) in lysis buffer (PBS containing 0.5% Triton X-100 and protease inhibitor) at 4 °C overnight. Radiolabeled proteins synthesized by *in vitro* translation with the TNT-coupled translation kit (Promega) or protein extracts from 293T cells overexpressing the target protein were incubated with GST-fusion protein at 4 °C for 2 h to overnight. The beads were washed three times with lysis buffer. Eluted proteins were separated by SDS/PAGE and detected by autoradiography or immunoblotting.

Co-immunoprecipitation assay (Co-IP). Cells were lysed with 50 mM Tris-HCl (pH 7.4) buffer containing 150 mM NaCl, 0.5% Triton X-100, 5 mM EDTA, 10% (vol/vol) glycerol, protease inhibitor, and phosphatase inhibitor at 4 °C for 30 min. Cell lysates were centrifuged, and the supernatants were incubated with a specific antibody at 4 °C for 4 h with gentle agitation, and protein A/G agarose beads were added for 2 h. After washing with cold lysis buffer three times, the precipitates were dissolved in the SDS sample buffer and subjected to SDS-PAGE.

Quantitative Real Time PCR (qRT-PCR). Transcript levels of CDK4, MRS, and Papola (endogenous control) were measured by qRT-PCR. RNA was extracted from cells using TRIzol (Thermo Fisher Scientific) following the manufacturer's instructions. A total of 2 μg of RNA was reverse-transcribed with M-MLV Reverse Transcriptase (Invitrogen) using random hexamers. The cycling conditions were 65 °C/5 min, 37 °C/2 min, 25 °C/10 min, 37 °C/50 min, and 70 °C/15 min to synthesize cDNA from the extracted RNA. qRT-PCR was performed with POWER SYBR GREEN master mix (Applied Biosystems) according to manufacturer's protocol. The primers 5'-GAGGATGGGAAATTCTCTAAGAGCCG-3' and 5'-TTGGTTGCCATGTCGAGATATGGTGAGGATACT-3' were used for MRS transcript detection, and 5'-ATGGCTACCTCTCGATATGAGCCA-3' and 5'-TCACTCCGGATTACCTTCATCCTT-3' were used for CDK4 transcript detection. Papola transcript was detected by using the primer set 5'-CACCAAGCC CACCCATTC-3' and 5'-AAACTTTTTGAAGCTCCAAACTTCTT-3'.

Met or Leu incorporation assay. Stable MDA-MB-231 cells whose sh-MRS was induced by doxycycline treatment and H460 cells transfected with si-MRS were seeded in 12-well plates and incubated. Primary MEF cells originated from WT, heterozygous, and homozygous *MARS* genetrap mice were also used. Media were changed to Met-free media (Welgene) containing [^{35}S]Met (PerkinElmer). After 2 h of incubation, cells were lysed, and the amount of radioactive protein was measured with a liquid scintillation counter (PerkinElmer).

To investigate translation under stress conditions, cancer cell lines were incubated with serum-free and Met-free media (Welgene) for 6 h, and then, the media were changed to Met-free media containing [^{35}S]Met or Leu-free media (Welgene) containing [^{3}H]Leu (American Radiolabeled Chemicals). After 30 min of incubation, cells were lysed, and the amount of radioactive protein was measured using a liquid scintillation counter (PerkinElmer).

ATP-PPi exchange assay. ATP-PPi exchange assay was performed as suggested by Uter *et al.* (*1*). The reaction mixture of the ATP-PPi exchange reaction was modified from a previously published reaction (*1*), consisting of 100 mM Tris-HCl (pH 7.5), 1 mM ATP, 5 mM PPi, 0.2 mM methionine, 5 mM $MgCl_2$, 10 mM KF, 0.1 mM EDTA, 0.1 mg/mL BSA, 10 mM β-mercaptoethanol, 0.22 mCi/mL γ-labeled [^{32}P]ATP, and 5% DMSO. The reaction was initiated with the addition of 1 μM MRS to varying concentrations of FSMO (0, 150, and 300 μM). The inhibitor was dissolved in 50% DMSO and tested at a final concentration of 5% DMSO in the reaction. An aliquot (1.5 μL) of each reaction was quenched with 3.0 μL of a solution consisting of 400 mM sodium acetate (pH 5.0) and 0.1% SDS. From this quenched reaction, 1.5 μL was spotted onto a polyethyleneimine cellulose plate that had been prewashed in water. The TLC plate was developed by buffer containing 750 mM KH_2PO_4 (pH3.5) and 4 M urea. The TLC plate was dried and exposed for 3 h to an image plate and quantified on a Typhoon 9400 variable mode imager (Amersham Biosciences).

Human cytoplasmic MRS expression and purification. Human MRS was purified according to a published method (*2*). The N-terminally truncated recombinant human cytoplasmic MRS was expressed from a 6 L culture of *E. coli* Rosetta2 strain harboring pET-MHs1 upon induction with 0.5 mM isopropyl β-D-1-thiogalactopyranoside (IPTG) at 25 °C overnight. Cells were disrupted by sonication in buffer containing 20 mM Tris-HCl pH 8.0, 100 mM NaCl, 8% (v/v) glycerol, 1.5 mg/mL lysozyme, 0.2 mM phenylmethylsulfonyl fluoride (PMSF) and 5 mM β-mercaptoethanol. The cell lysate was spun for 30 min at 10,000 × *g* and the supernatant was bound to TALON metal affinity resin (Clontech). The bound protein was eluted from the resin with the

sonication buffer containing imidazole, ranging from 10 to 800 mM, and the fractions with high purity (25-400 mM imidazole fractions) were combined and concentrated using Amicon ultra centrifugal filters (Millipore).

DARTS (drug affinity responsive target stability). Five micrograms of purified His-MRS (221-900 aa) protein and BSA (bovine serum albumin, Pierce) was mixed at a 1:2 molar ratio with FSMO and incubated at 25 °C for 30 min and then treated with 2 or 4 μg of Trypsin (Hyclone) for 5 min at RT. Each reaction was terminated by mixing with 2X SDS sample buffer and then loaded into SDS-PAGE gel. After electrophoresis, the gel was stained with Instant blue (Expedeon).

Modeling for the complex of MRS and CDK4. With the crystal structures of human MRS (PDB Id. 5GL7) and CDK4 (PDB Id. 2W96), we docked CDK4 on MRS manually using a program, Coot (*3*) to satisfy the specific interaction of MRS with CDK4 revealed from *in vitro* pull down assay, and to match prominence and depression on their binding surface. The binding interfaces were evaluated by calculation of contact areas in various distances between two proteins based on the binding direction (*4*). The possibility of the binding interface was confirmed using a docking program, Z-dock server (*5*). The residues in the binding interfaces were analyzed with program PISA (*6*).

Anchorage-independent soft agar assay. Base agar mixture (1 mL) containing 0.6% low-melting agarose was added into each well of 12 well plate and incubated at RT for 30 min to solidify. After incubation, stable MDA-MB-231 cells (3×10^3 cells/well) were mixed with equal volumes of 0.6% low-melting agarose containing 10% serum DMEM and then added onto the base agar. To monitor the anchorage-independent cell growth, 10% DMEM with doxycycline (1 μg/mL) was added into each well. After 1 month of incubation, the cells were fixed with 10% methanol/10% acetic acid for 10 min and then stained with 0.01% crystal violet for 1 h.

***In vivo* xenograft experiments.** Animal experiments complied with the University Animal Care and Use Committee guidelines at Seoul National University. Stable sh-Control (sh-Cont) and sh-MRS MDA-MB-231 cells expressing GFP (1×10^6 cells) were inoculated subcutaneously into the flanks of 6-week-old BALB/c Slc-*nu* SP nude female mice (n = 5/group). To induce siRNA expression, mice were supplied with doxycycline hydrochloride via drinking water (5% sucrose, 2 mg/mL). Mice were monitored every day and tumor volumes and body weights were checked every 3 d. After 3 weeks, Fluorescence from tumor regions was imaged using Optix MX3 (ART) and the mice were sacrificed. Tumor weights were measured and subjected to IHC staining.

Preparation of tissue microarray blocks. Formalin-fixed, paraffin-embedded tissue blocks were arrayed using an Accu Max Array tissue-arraying instrument (Petagen, Inc, Korea). Briefly, representative areas of each tumor were selected and marked on the H&E slide by breast pathologists. The designated zone of each donor block was punched with a tissue cylinder 3 mm in diameter, and the sample was transferred to a recipient block in a grid pattern.

IHC staining. Paraffin-embedded sections were prepared at a 4-mm thickness followed by the standard H&E staining. Additional sections were manually deparaffinized in xylene and rehydrated in a series of graded ethanol solutions. After deparaffinization and rehydration, the sections were treated with a 3% (v/v) hydrogen peroxide solution for 10 min to block endogenous peroxidase and pretreated for antigen retrieval in Epitomic retrieval solution 2, pH 6.0, from Leica Biosystems (Melbourne, Australia) at 100 °C for 20 min. After incubation with primary antibodies against MRS (NMS-01-0003, Neomics), p16 (JC8, Santa Cruz), cyclin D1 (H295, Santa Cruz), CDK4 (C-22, Santa Cruz), and pRb (ER182N, Abcam), the sections were subjected to staining using an automated Leica Bond-max immunostainer (Leica Biosystems) according to the manufacturer's instructions. Stained tissue images were captured on a Nikon TE2000 inverted microscope with IP Lab software (BD Biosciences Clontech; Palo Alto, CA). Slides were counterstained with Harris

hematoxylin. Normal breast tissue entrapped within the block and appropriate control tissues were used as positive controls. Archival H&E stained slides for each case were reviewed by a pathologist who is an expert in breast pathology. For interpretation of the IHC stain results, the IHC tests for MRS, p16, cyclin D1, CDK4, and pRb were graded from 0 to 100 and categorized as negative “0 (< 25),” ‘‘1+ (25-50),’’ ‘‘2+ (50-75),’’ or ‘‘3+ (>75)’’ in high-power fields according to the intensity of staining in each case. High expression of MRS was assigned for scores ‘‘2+’’ and ‘‘3+.’’ High expression of other markers was assigned for scores “1+ - 3+.” The interpretation of IHC results was carried out blindly, without any information regarding clinical parameters or outcome. For WSS generation, refer to Table S2.

References

1. Uter, N. T., Gruic-Sovulj, I., and Perona, J. J. (2005) Amino acid-dependent transfer RNA affinity in a class I aminoacyl-tRNA synthetase, *J. Biol. Chem. 280*, 23966-23977. DOI: 10.1074/jbc.M414259200.
2. Kaminska, M., Shalak, V., and Mirande, M. (2001) The appended C-domain of human methionyl-tRNA synthetase has a tRNA-sequestering function, *Biochemistry. 40*, 14309-14316.
3. Emsley, P., and Cowtan, K. (2004) Coot: model-building tools for molecular graphics, *Acta Crystallogr. D. 60*, 2126–2132. DOI: 10.1107/S0907444904019158
4. Kang, B. S., Pugalendhi, G., and Kim, K. (2017) Binding direction-based two-dimensional flattened contact area computing algorithm for protein-protein interactions, *Molecules 22*, E1722. DOI: 10.3390/molecules22101722
5. Pierce, B. G., Wiehe, K., Hwang, H., Kim, B. H., Vreven, T., and Weng, Z. (2014) ZDOCK server: Interactive docking prediction of protein-protein complexes and symmetric multimers, *Bioinformatics 30*, 1771-1773. DOI: 10.1093/bioinformatics/btu097
6. Krissinel, E., and Henrick, K. (2007) Inference of macromolecular assemblies from crystalline state, *J. Mol. Biol. 372*, 774--797. DOI: 10.1016/j.jmb.2007.05.022

Supplementary Figures

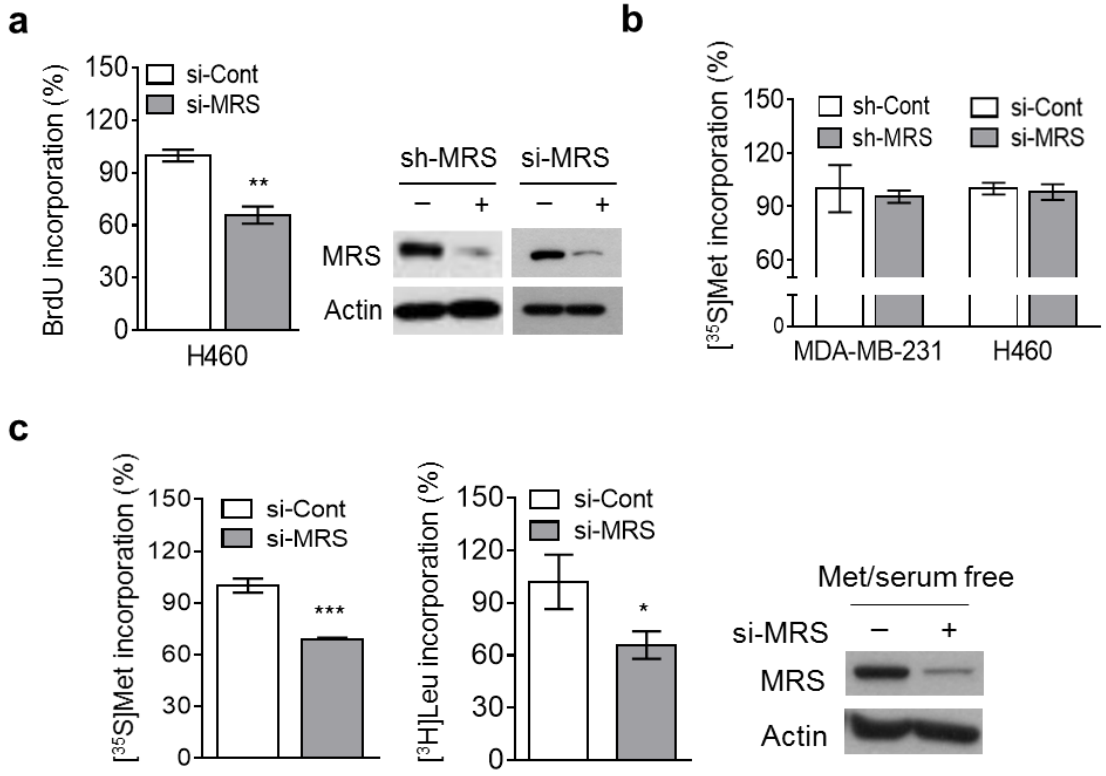

Figure S1. Effect of MRS on global translation in cancer cell lines. (a) DNA synthesis in H460 cells in which the MRS level reduced by si-RNA transfection was detected using BrdU incorporation assay (left, mean ± SD, $n = 3$). **, $P < 0.01$. The MRS level was monitored via immunoblotting in MDA-MB-231 and H460 cells whose MRS level was reduced by sh-MRS and si-MRS expression, respectively (right). (b) Global protein synthesis was monitored via [^{35}S]Met incorporation in the stable MDA-MB-231 expressing inducible sh-MRS or si-MRS transfected H460 cells (mean ± SD, $n = 3$). (c) Global protein synthesis was monitored via [^{35}S]Met incorporation (left) and [^{3}H]Leu incorporation (middle). H460 cells were transfected with si-MRS and incubated with serum-free media with Met deprivation. The reduced level of MRS following si-MRS transfection was investigated via immunoblotting (right) (mean ± SD, $n = 3$). *, $P < 0.05$; ***, $P < 0.001$.

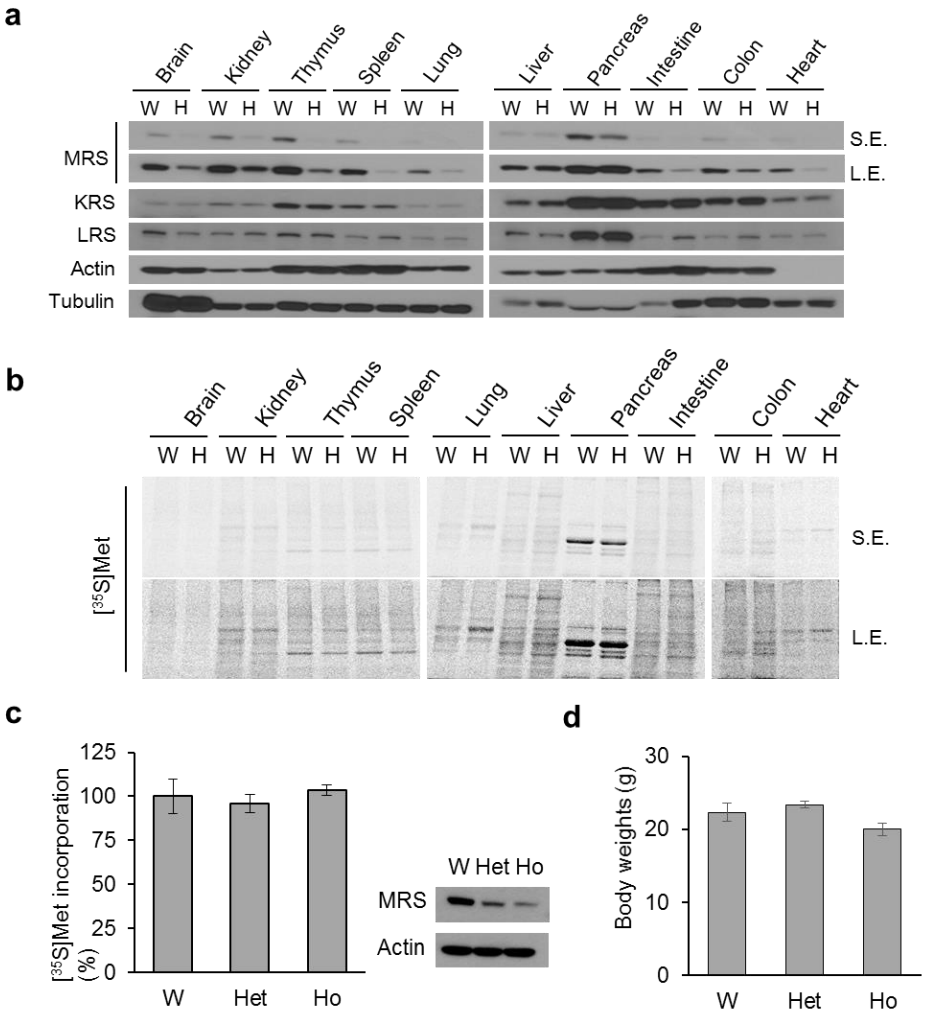

Figure S2. Effect of MRS knockdown on global translation *in vivo*. (a-b) The MRS level (a) and global protein synthesis (b) in each organ from the wild type (W) and homozygous (H) mice were compared via immunoblotting and [^{35}S]Met incorporation, respectively. KRS (lysyl-tRNA synthetase), LRS (leucyl-tRNA synthetase), actin, and tubulin were used as controls. S.E., short exposure; L.E., long exposure. (c) Global protein synthesis was monitored via [^{35}S]Met incorporation in the primary MEF cells originated from wild type (W), heterozygous (Het), and homozygous (Ho) mice (left, *n* = 2). The MRS level was also detected from the primary MEF cells (right). There was no significant difference in the [^{35}S]Met incorporation level in (c). (d) The body weights in W, Het, and Ho mice at 6 weeks old (*n* = 3) were investigated. There was no significant difference in the body weights.

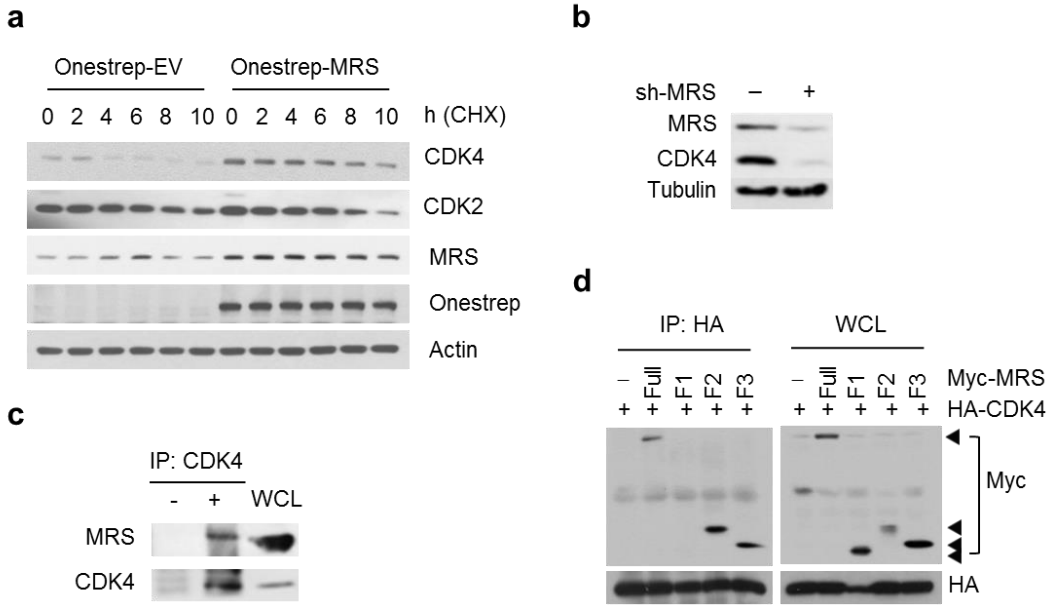

Figure S3. MRS specifically regulates and interacts with CDK4. (a) Specific stabilization of CDK4 levels by Strep-MRS-transfection into MDA-MB-231 cells treated with cycloheximide (CHX, 120 μg/mL). (b) The level of MRS and CDK4 in the stable MDA-MB-231 cells after sh-MRS induction was monitored via immunoblotting. (c) Interaction between endogenous MRS and CDK4 was monitored by immunoprecipitation. (d) Interaction between Myc-MRS fragments (F1-F3 in Figure 2c) and HA-CDK4 expressed in H460 cells was determined by co-immunoprecipitation.

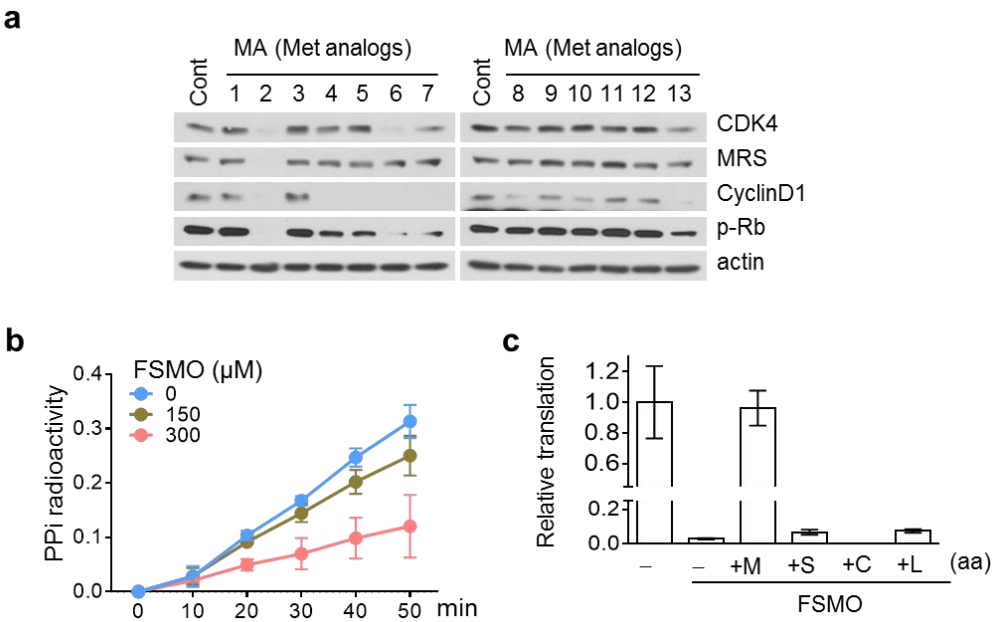

Figure S4. The specific Met analog FSMO regulates MRS-mediated CDK4 stability mimicking MRS knockdown. (a) MDA-MB-231 cells were treated with Met analogs, and their effects on CDK4 were detected via immunoblotting. (b) FSMO effect on the Met-activation reaction by the ATP-PPi exchange assay (mean ± SD, *n* = 2). (c) Excess amino acids (aa, 25 mM) were added into the luciferase-based *in vitro* translation system and the recovery effect of translation inhibited by FSMO (1 mM) was analyzed. M, methionine; S, serine; C, cysteine; L, leucine (mean ± SEM, *n* = 3).

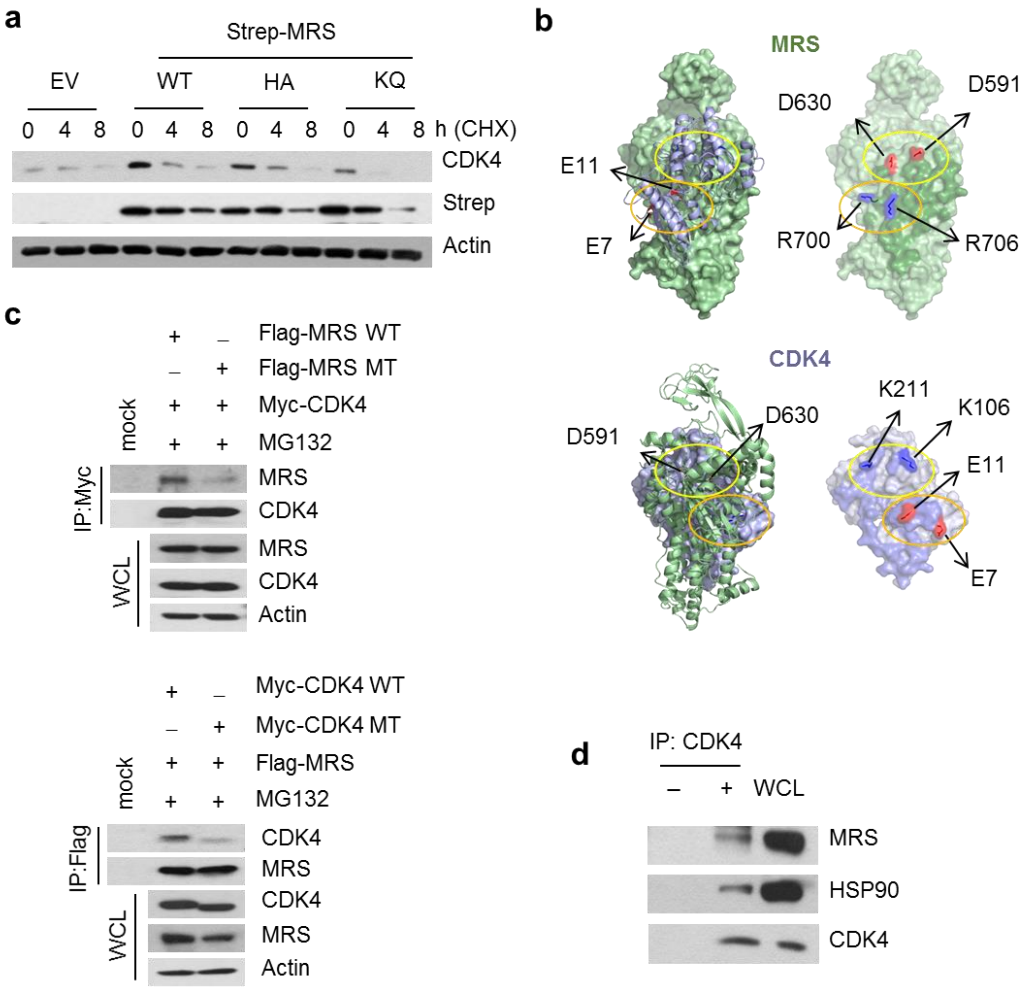

Figure S5. MRS interacts with CDK4 and HSP90. (a) Strep-MRS WT and H560A (HA), but not the K596Q (KQ) mutant, stabilized CDK4 under CHX-treated conditions. (b) Residues at the binding interfaces of MRS (pale green, upper) and CDK4 (light blue, lower) that may be involved in electrostatic interactions based on the docking model. Residues (sticks, red or blue color for negative or positive charge, respectively) are in the binding area (dark color) on the surfaces of proteins (right), and the binding partners are presented as a ribbon diagram (left). (c) Interaction of a Flag-MRS dual mutant (MT), D591R/D630R, with Myc-CDK4 (upper) and that of Myc-CDK4 MT, E7R/E11R, with Flag-MRS (lower) were investigated via immunoprecipitation, under MG132-treated conditions. (d) Endogenous co-immunoprecipitation among MRS, CDK4, and HSP90.

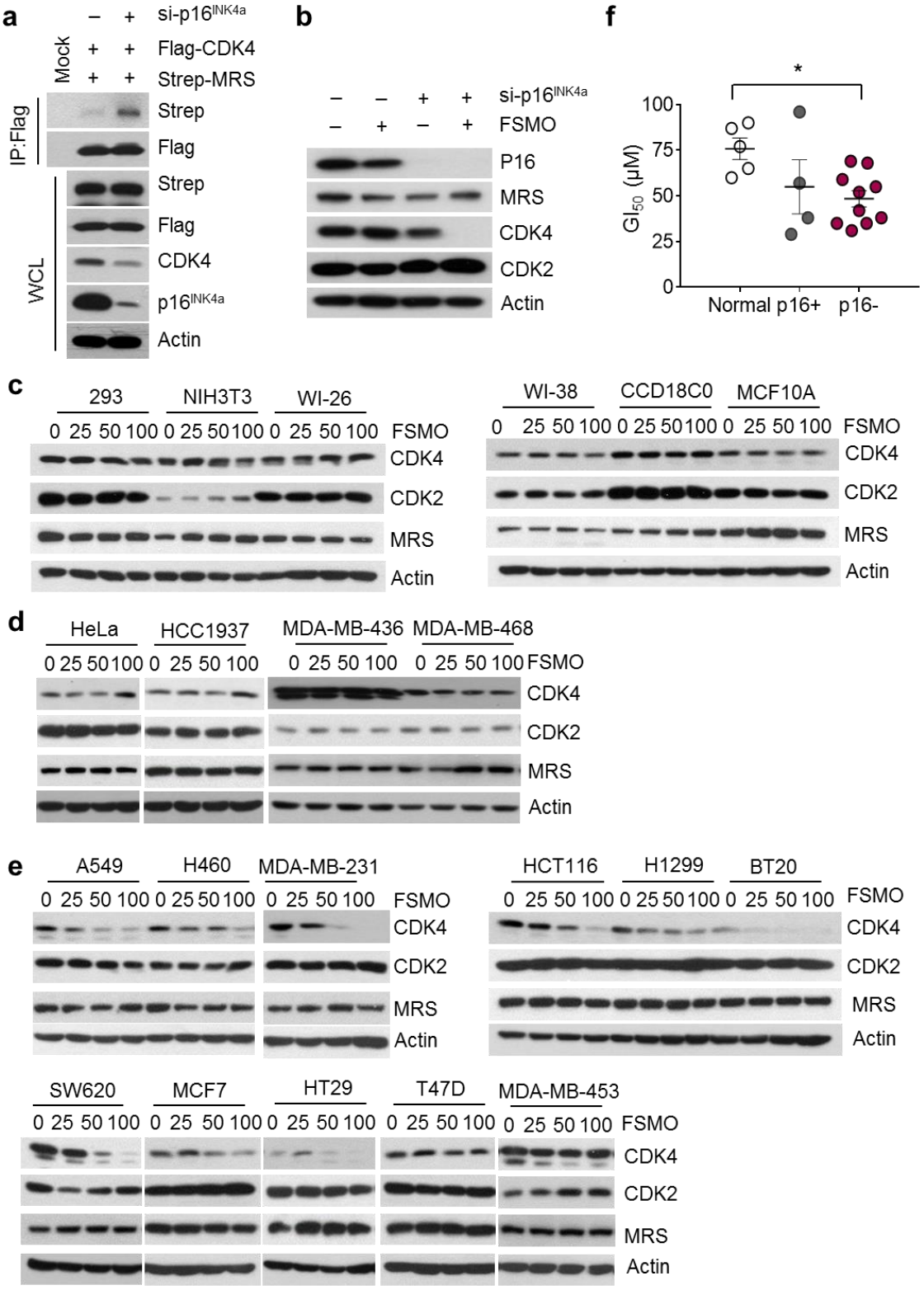

Figure S6. Effect of MRS on CDK4 is dependent on p16^{INK4a} status. (a) Effect of p16^{INK4a} knockdown on the interaction between Flag-CDK4 and Strep-MRS in WI-26

cells. (b) Effect of FSMO on CDK4 with or without $p16^{INK4a}$ knockdown in WI-26 cells. (c-e) Normal cells (c), $p16^{INK4a}$-positive cancer cells (d), and $p16^{INK4a}$-negative cancer cells (e) were treated with FSMO at the indicated concentration for 9 h, and then, the levels of CDK4, CDK2, and MRS were detected by immunoblotting. CDK4 was detected in two bands in MDA-MB-436, SW620, and MDA-MB-453 cells, and both bands were included in the quantification. (f) The GI_{50} values (the concentration for 50% of maximal inhibition of cell proliferation) of FSMO in the normal, $p16^{INK4a}$-positive cancer cells and $p16^{INK4a}$-negative cancer cells were determined. *, $P < 0.05$.

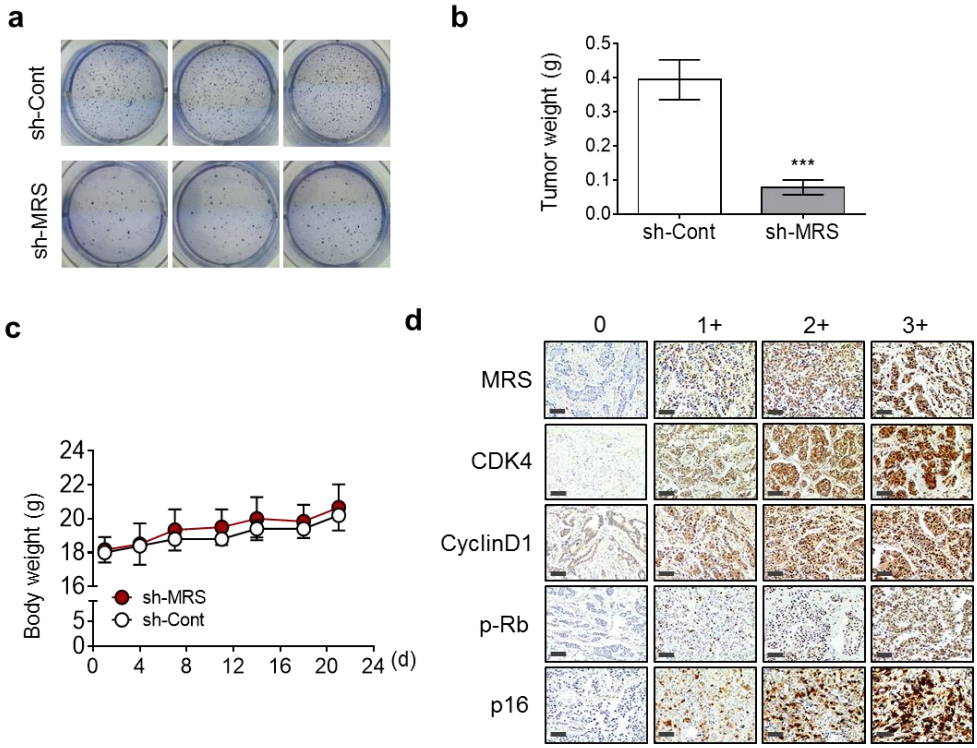

Figure S7. Effect of MRS suppression on tumor growth and the correlation between MRS and CDK4 in breast cancer patients. (a) Anchorage-independent soft agar assay was performed with stable MDA-MB-231 cells with sh-control (sh-Cont) and sh-MRS. (b-c) Stable MDA-MB-231 cells expressing GFP and inducible sh-MRS were inoculated for a xenograft experiment. Tumor weights (b) and the mouse body weights (c) are shown. ***, $P < 0.001$ (mean ± SEM, $n = 10$). (d) IHC staining was performed using a breast cancer TMA array to detect the levels of MRS, CDK4, cyclin D1, pRb (S780), and $p16^{INK4a}$. Staining intensity for each protein was categorized as "0," "1+," "2+," or "3+." Bar = 50 μm. A representative IHC image for the grade is shown.

Supplementary Tables

Table S1. Met analogues (MA) used in this study.

No.	Met analogs (MA)
1	Di-Fmoc-L-homocystine
2	Boc-S-trityl-L-homocysteine
3	Boc-DL-methionine methylsulfonium chloride
4	Fmoc-DL-selenomethionine
5	Fmoc-DL-ethionine
6	Fmoc-Sec(Mob)-OH
7	Fmoc-α-methyl-DL-methionine
8	Fmoc-DL-methionine methylsulfonium chloride
9	Boc-DL-buthioninesulfoximine
10	Boc-DL-ethionine
11	Fmoc-DL-buthioninesulfoximine
12	Boc-DL-selenomethionine
13	Boc-α-methyl-DL-methionine

Table S2. Criteria for the additional points (AP) and WSS (weighted sum of score).

IHC score			AP	WSS	IHC score			AP	WSS
CDK4	Cyclin D1	pRb			CDK4	Cyclin D1	pRb		
0	0	0	-1	-1	2	0	0	-1	1
		1	0	1			1	0	3
		2	1	3			2	1	5
		3	2	5			3	2	7
	1	0	1	2		1	0	1	4
		1	2	4			1	2	6
		2	3	6			2	3	8
		3	4	8			3	4	10
	2	0	2	4		2	0	2	6
		1	3	6			1	3	8
		2	4	8			2	4	10
		3	5	10			3	5	12
	3	0	3	6		3	0	3	8
		1	4	8			1	4	10
		2	5	10			2	5	12
		3	6	12			3	6	14
1	0	0	-1	0	3	0	0	-1	2
		1	0	2			1	0	4
		2	1	4			2	1	6
		3	2	6			3	2	8
	1	0	1	3		1	0	1	5
		1	2	5			1	2	7
		2	3	7			2	3	9
		3	4	9			3	4	11
	2	0	2	5		2	0	2	7
		1	3	7			1	3	9
		2	4	9			2	4	11
		3	5	11			3	5	13
	3	0	3	7		3	0	3	9
		1	4	9			1	4	11
		2	5	11			2	5	13
		3	6	13			3	6	15

To observe the sequential flow of signal activation within MRS-CDK4-cyclin D1-pRb, additional points (AP) were added to the sum of score of CDK4-Cyclin D1-pRb, which was obtained from the IHC staining of breast cancer TMA. By adding the AP value to the sum of IHC score, the WSS (weighted sum of score) was obtained, and its dependency on the MRS level as well as $p16^{INK4a}$ was analyzed. For example, a case whose IHC scores for CDK4, cyclin D1 and pRb are 1, 0 and 0, respectively, gets a "-1" value for AP because the sequential flow of signal activation is not indicated. Another case whose IHC scores for CDK4, cyclin D1 and pRb are 1, 1 and 0, respectively, gets a "1" AP value because small sequential flow of signal activation is

observed, resulting in a WSS score of “3.” The AP value is introduced to evaluate the sequential activation flow. Without AP, the sum of score of CDK4-cyclin D1-pRb cannot distinguish 1-1-0 from 1-0-1, the former represents sequential activation from CDK4 to cylcin D1 although it was not linked to pRb, while the latter indicates the unrelated activation of pRb.

Raw Data for Immunoblotting

Figure 1. MRS inhibition induces G1 cell cycle arrest via specifically reducing CDK4 level and its downstream signaling.

C MDA-MB-231

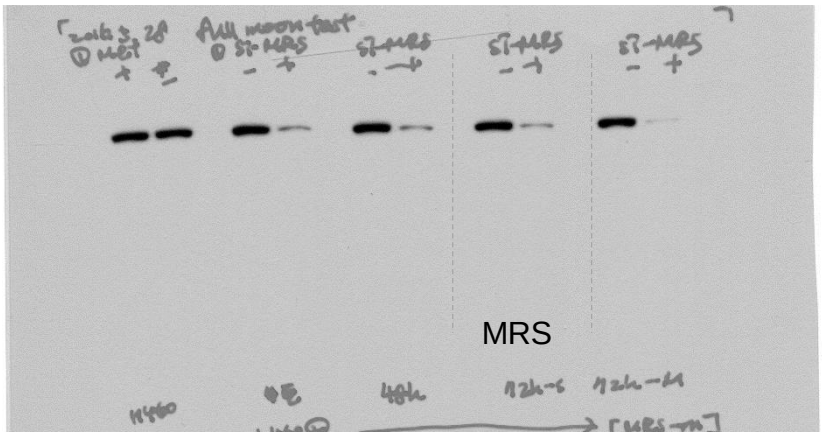

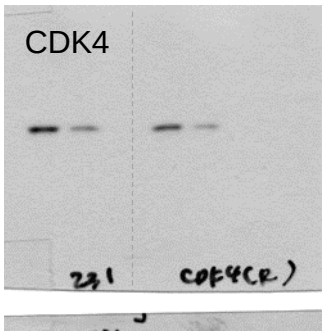

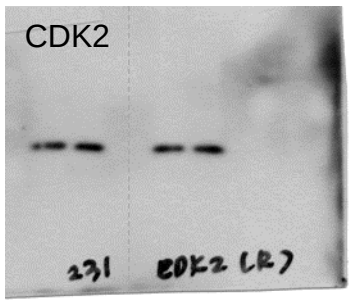

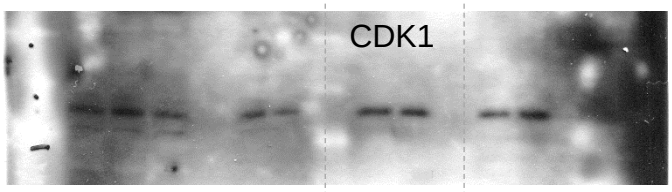

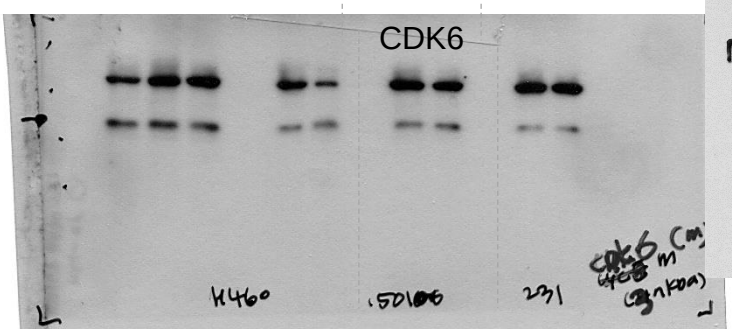

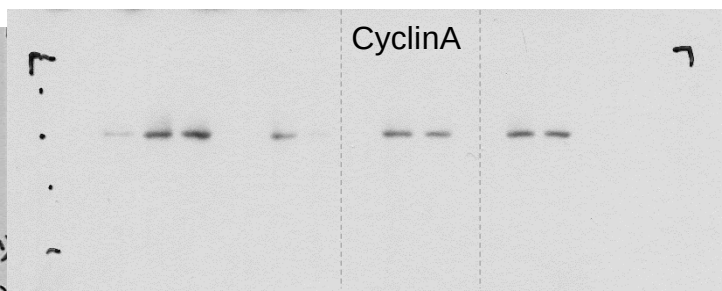

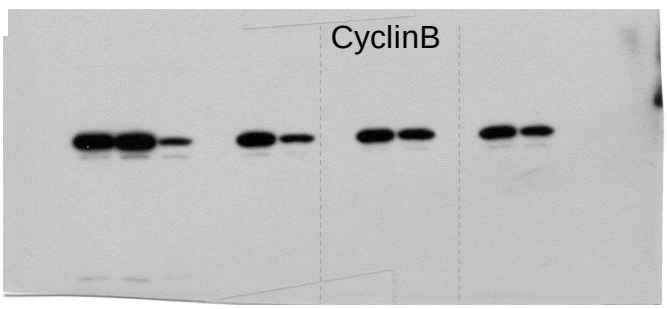

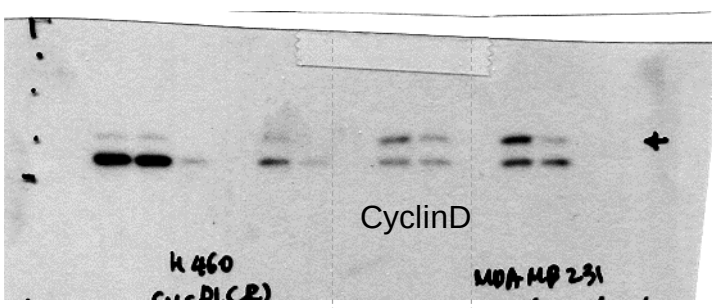

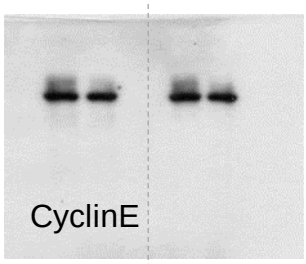

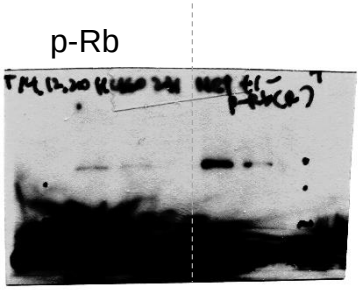

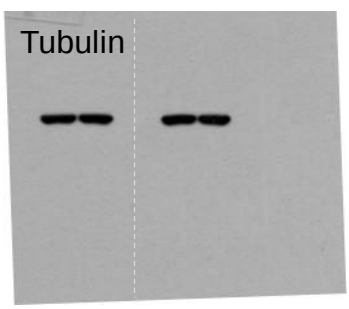

Figure 1. MRS inhibition induces G1 cell cycle arrest via specifically reducing CDK4 level and its downstream signaling.

C H460

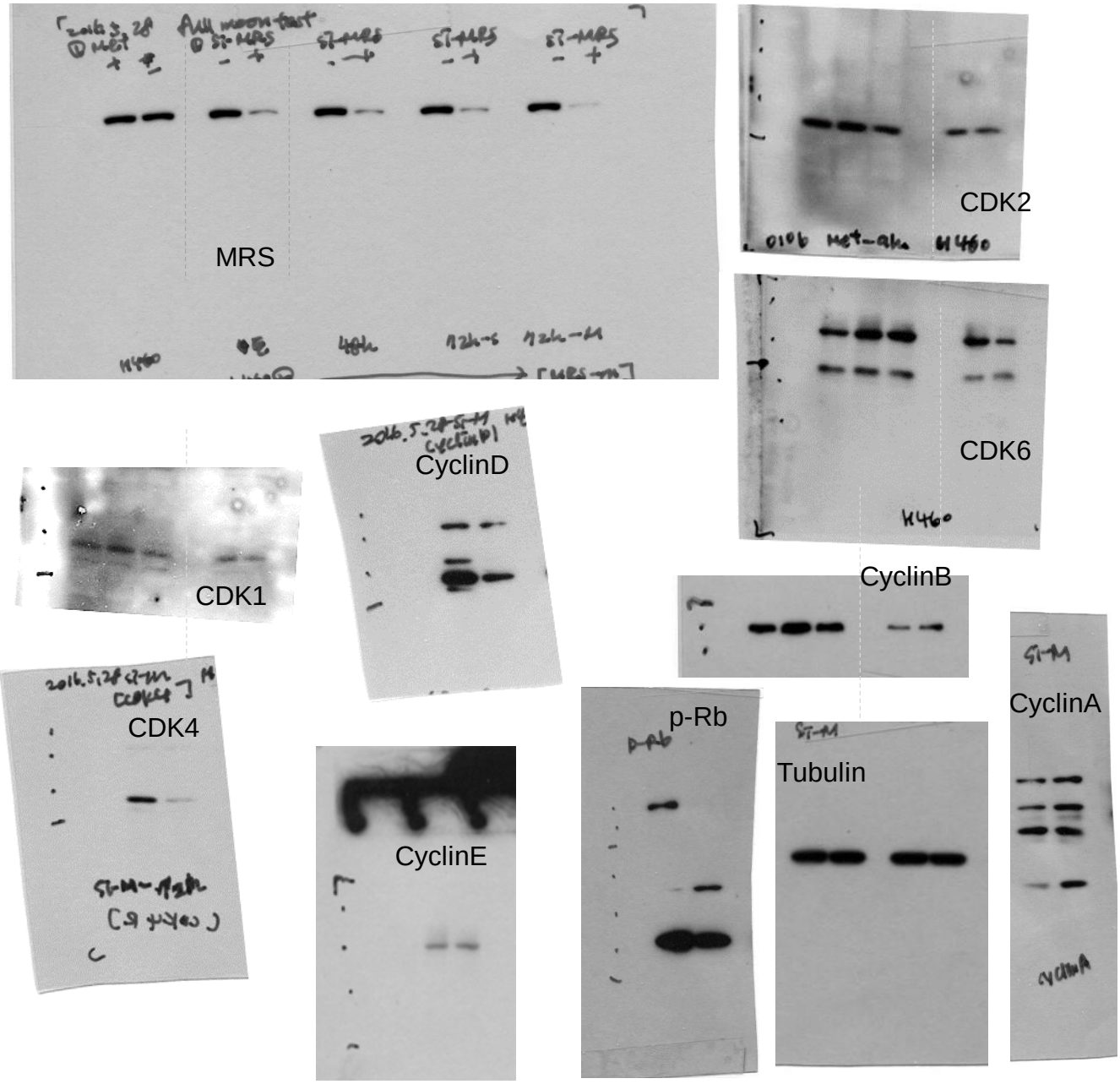

Figure 1. MRS inhibition induces G1 cell cycle arrest via specifically reducing CDK4 level and its downstream signaling.

d

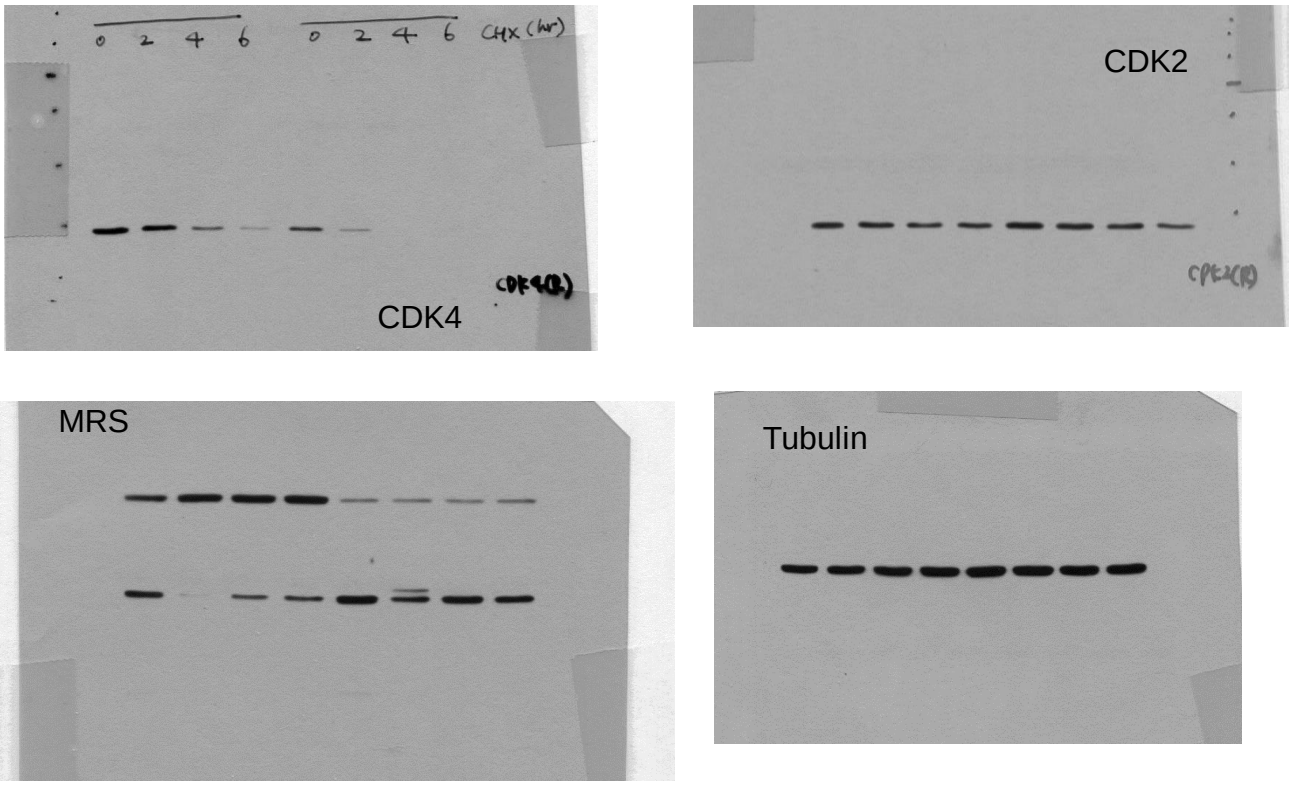

Figure 3. MRS inhibition induces G1 cell cycle arrest via specifically reducing CDK4 level and its downstream signaling

b

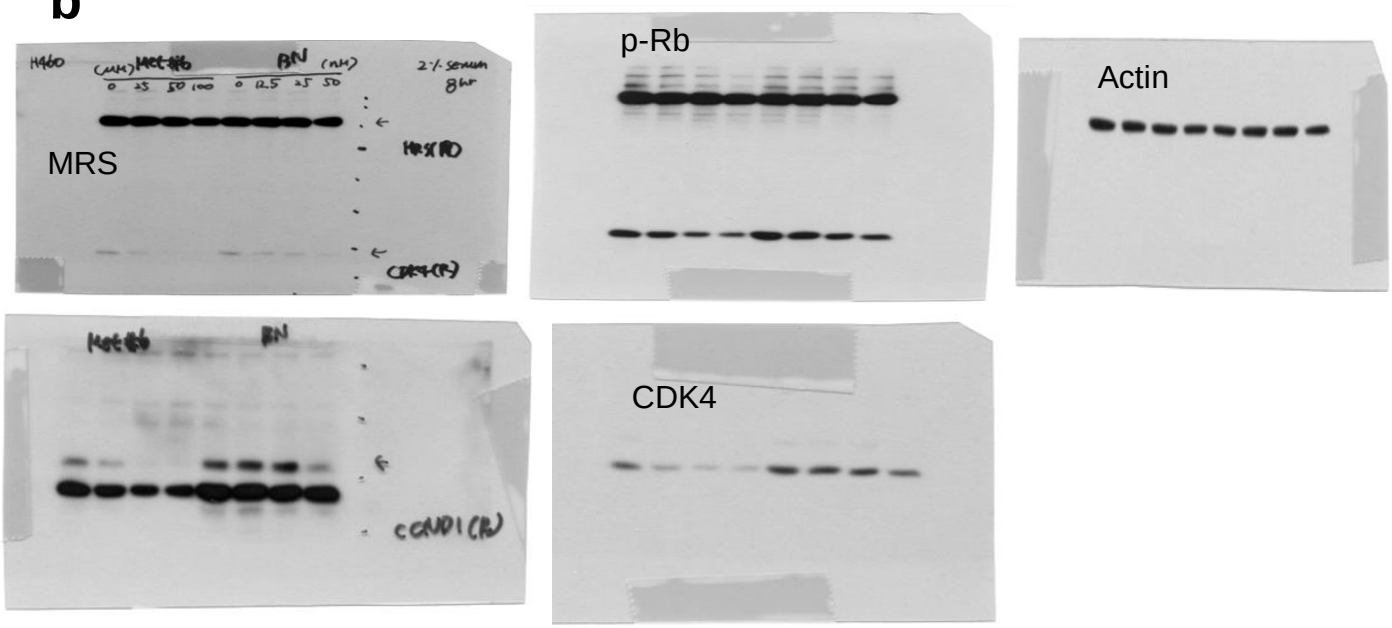

Figure 3. MRS inhibition induces G1 cell cycle arrest via specifically reducing CDK4 level and its downstream signaling.

e

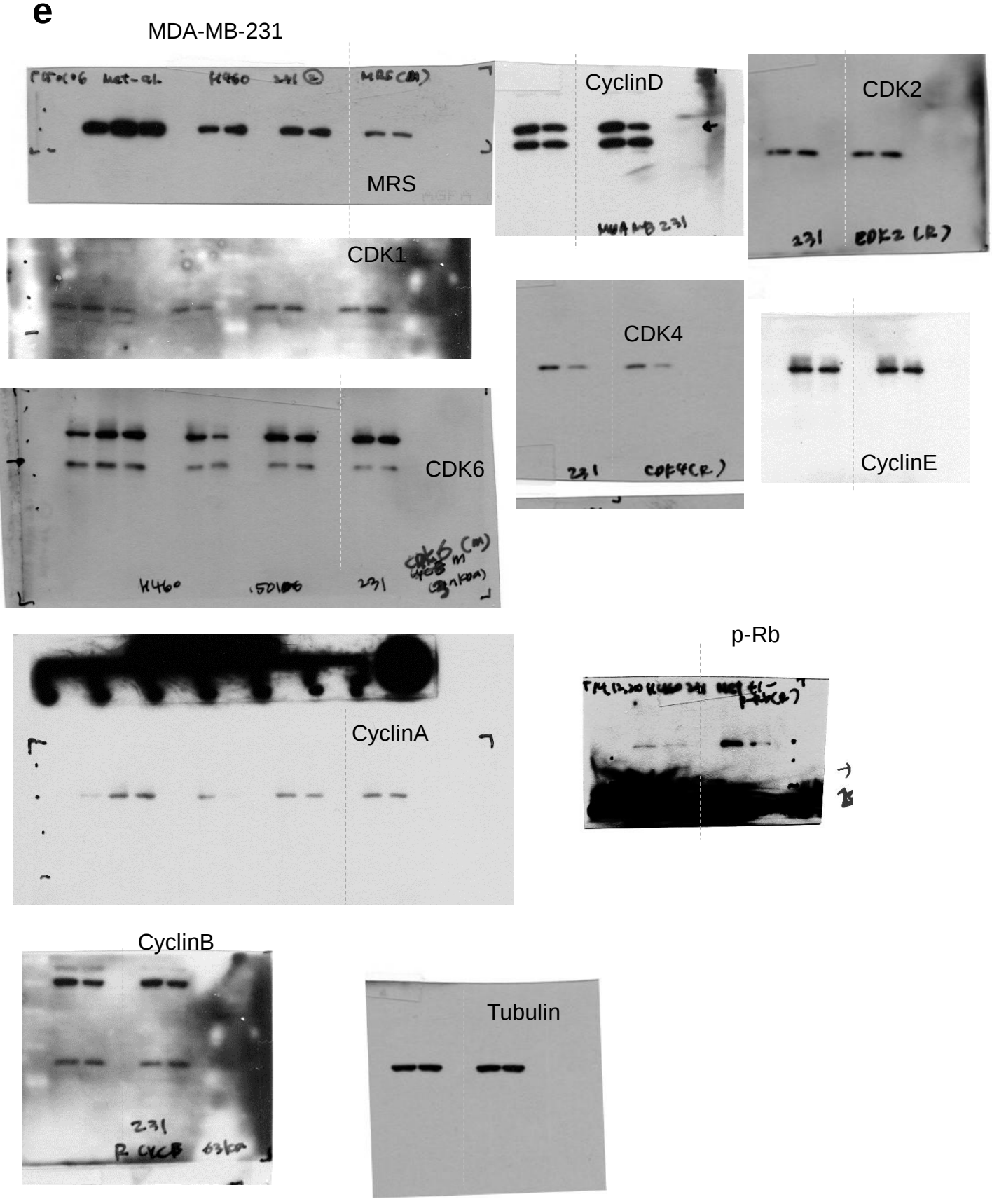

Figure 3. MRS inhibition induces G1 cell cycle arrest via specifically reducing CDK4 level and its downstream signaling.

e H460

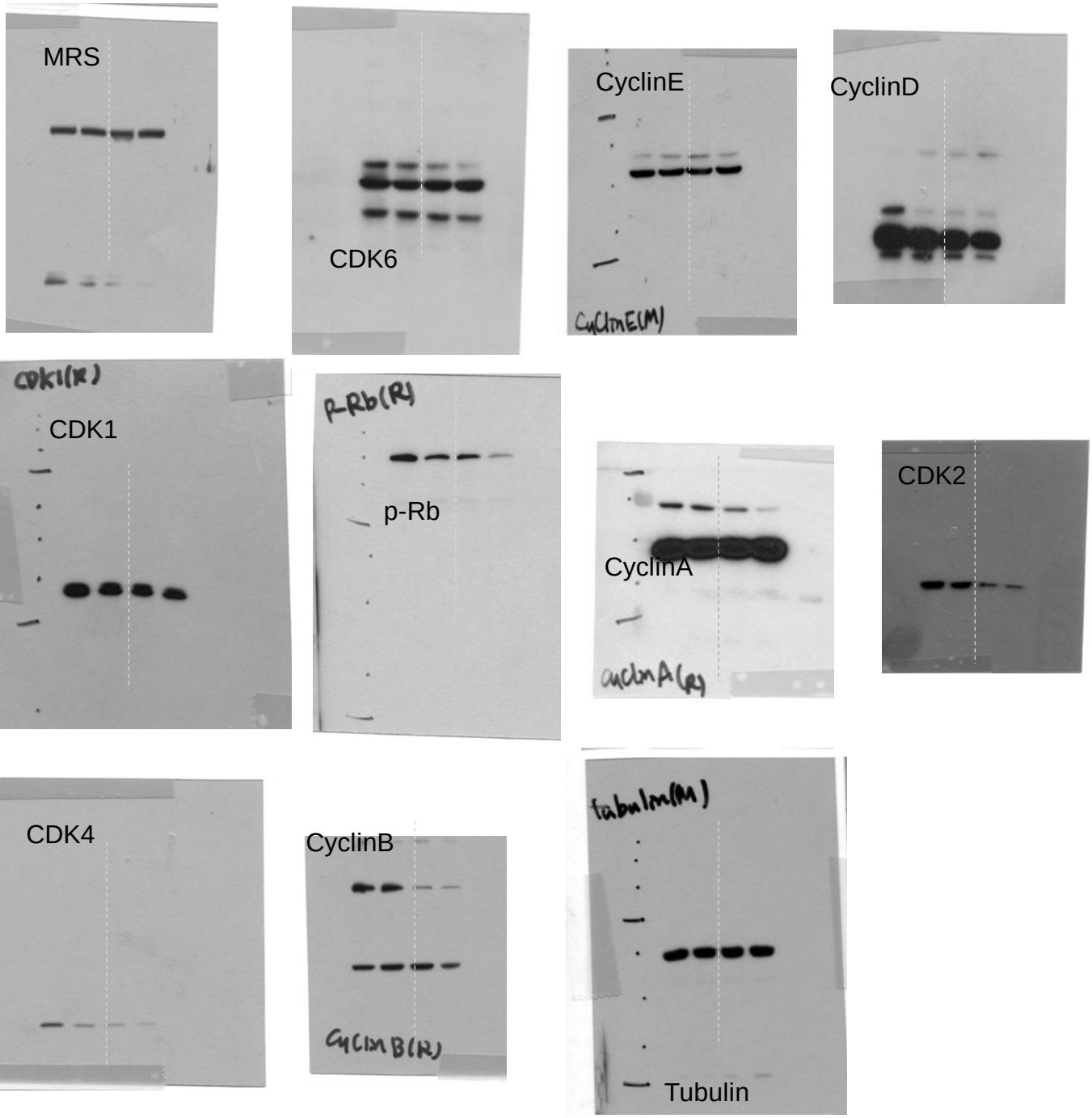

Figure 3. MRS inhibition induces G1 cell cycle arrest via specifically reducing CDK4 level and its downstream signaling.

h

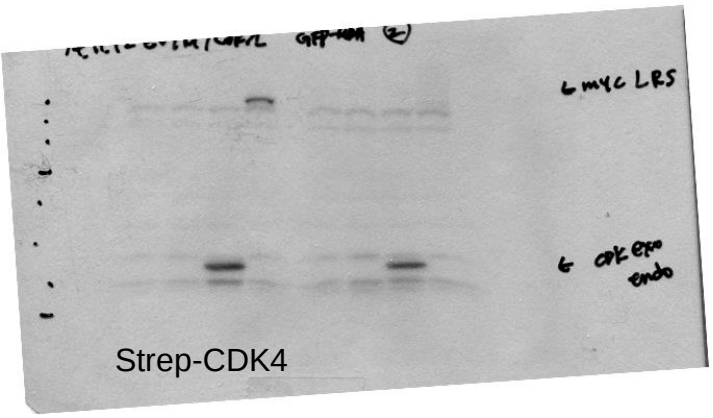

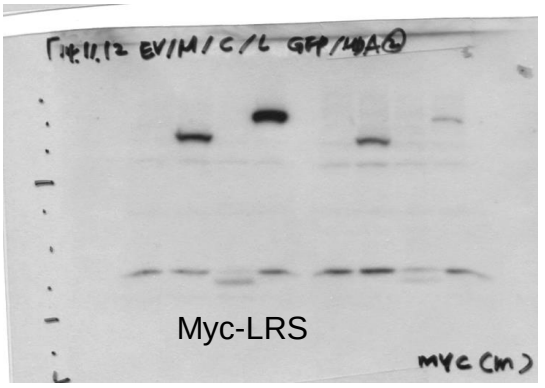

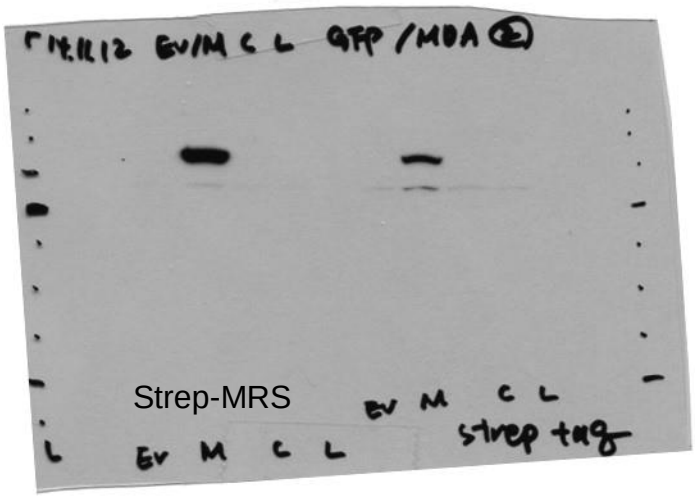

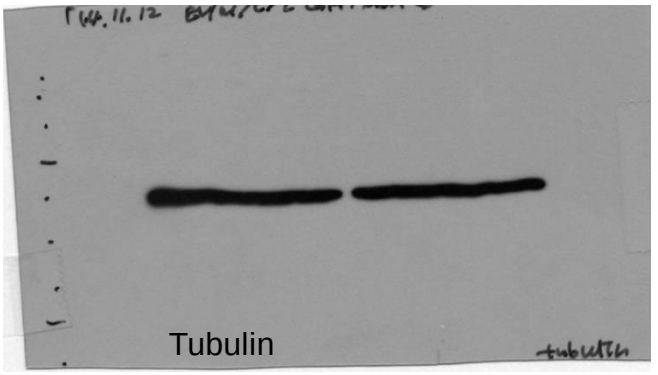

Figure 4. FSMO shares the binding site of MRS with CDK4.

a

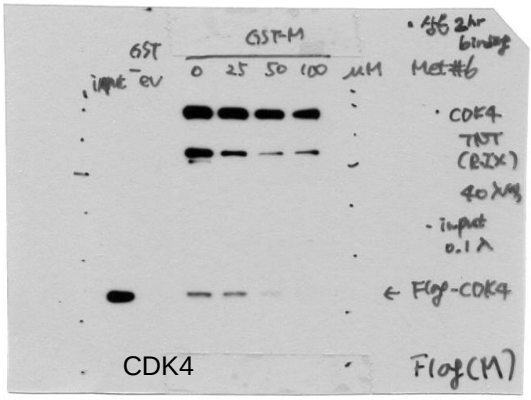

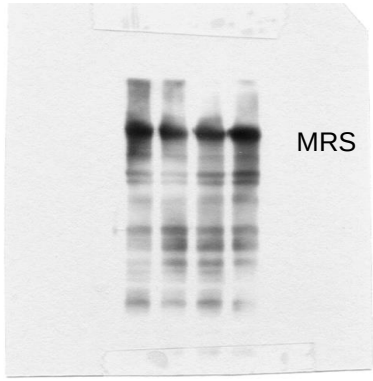

b

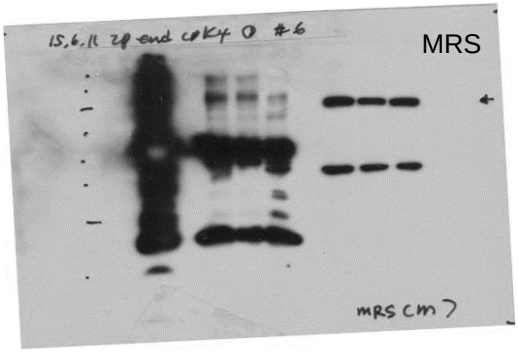

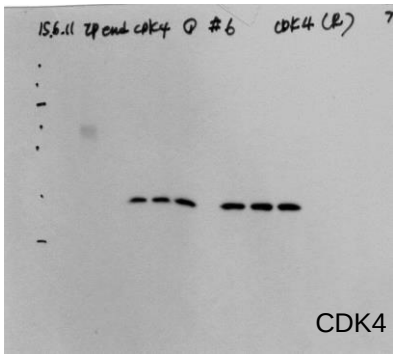

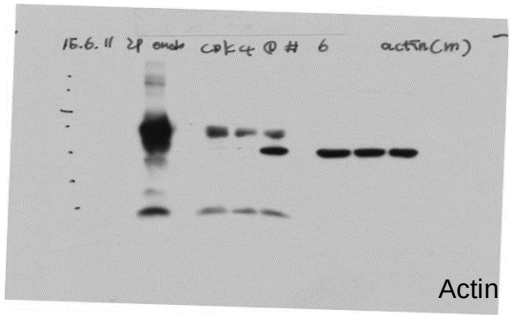

C

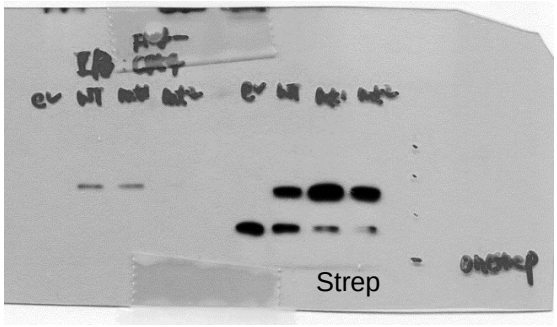

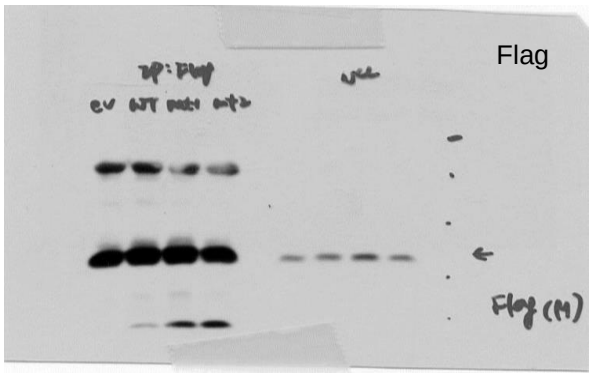

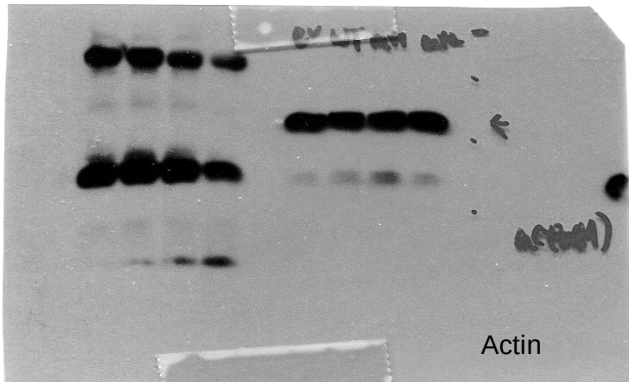

Figure 5. MRS facilitates CDK4 and Hsp90 complex formation and stabilizes CDK4.

a

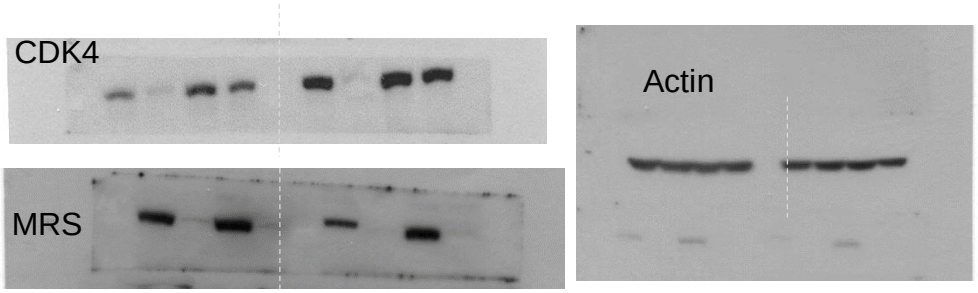

b

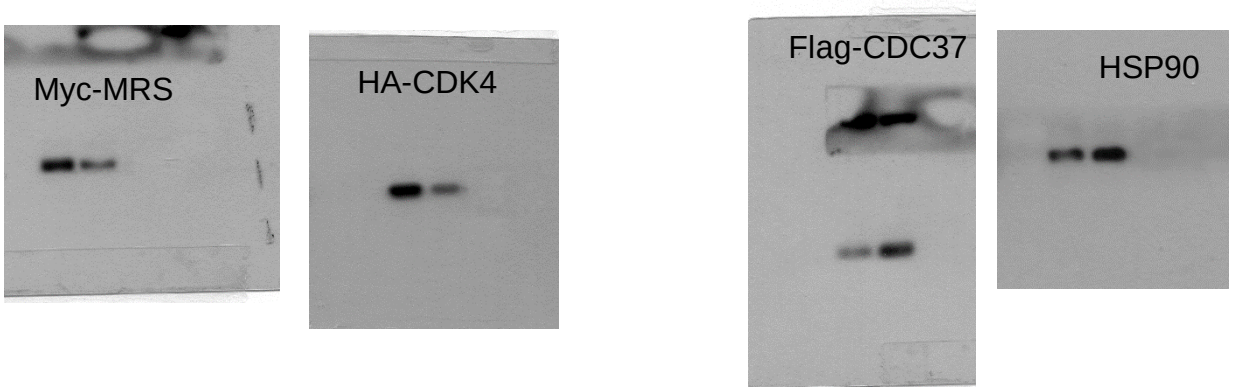

Figure 5. MRS facilitates CDK4 and Hsp90 complex formation and stabilizes CDK4.

d

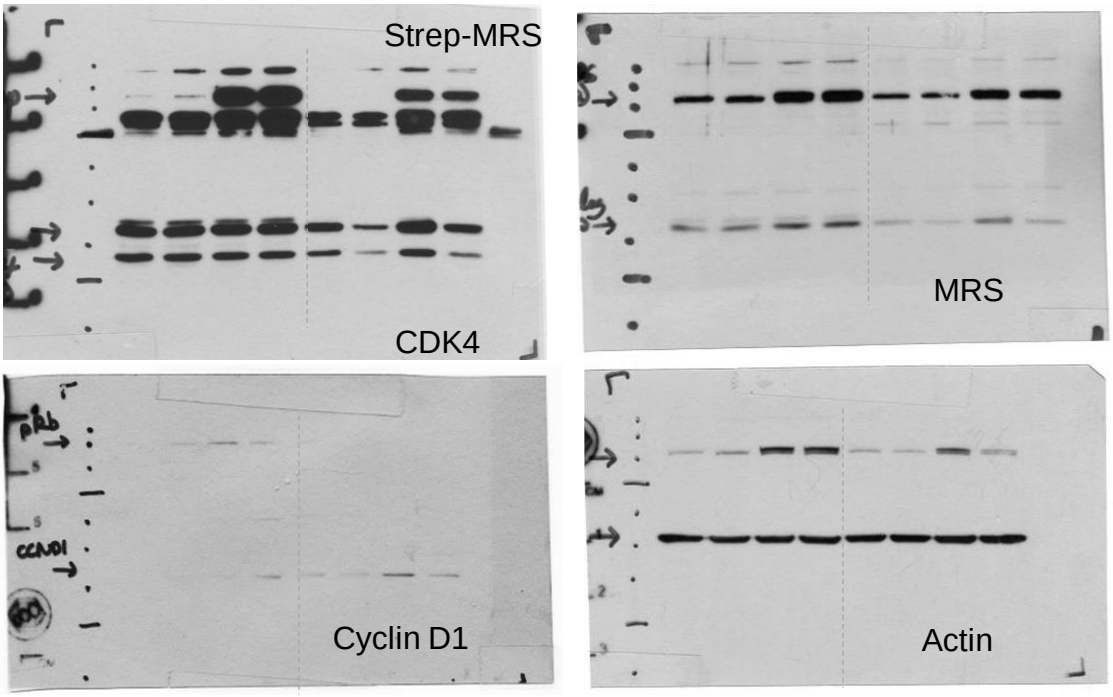

f

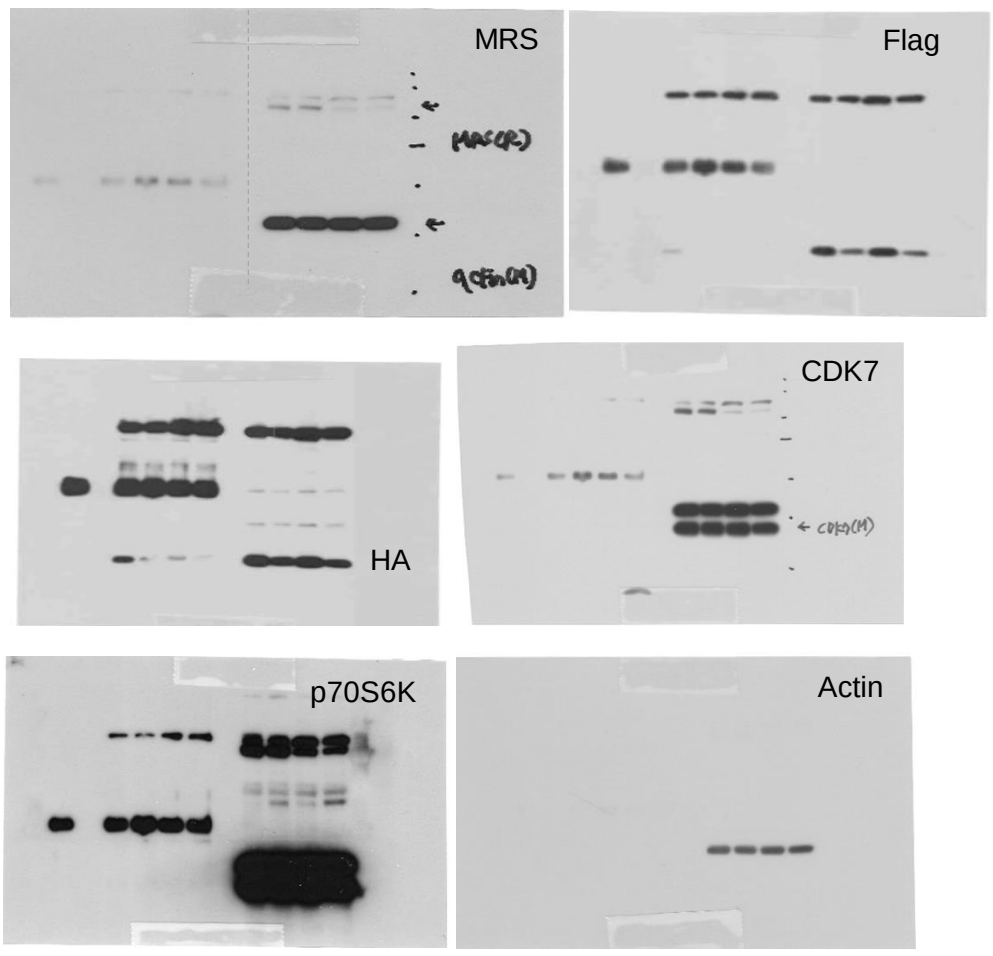

Figure 6. MRS shares interaction site with p16^{INK4a} for the binding to CDK4 but does not disturb the function of CDK4.

a

Input and GST

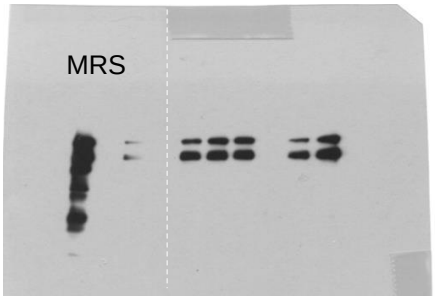

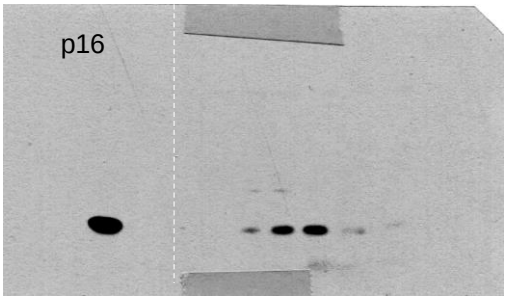

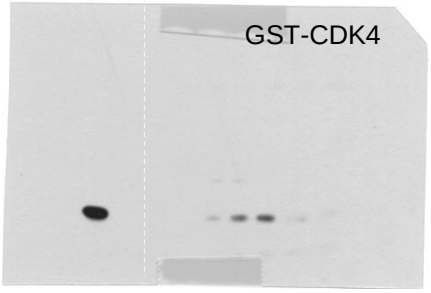

GST-CDK4 panel by adding different doses of MRS

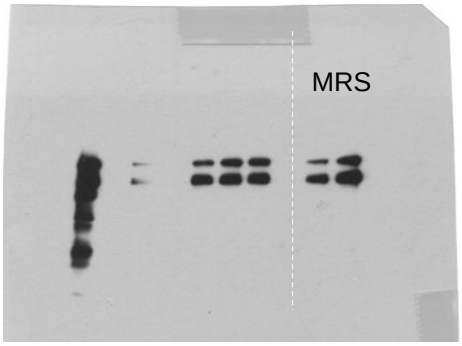

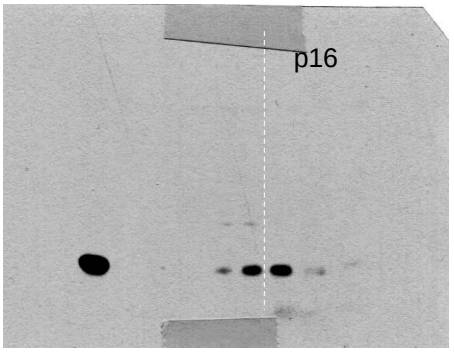

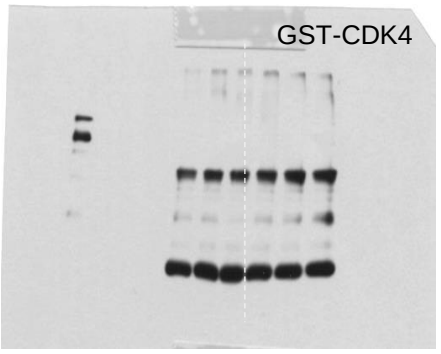

GST-CDK4 panel by adding different doses of p16

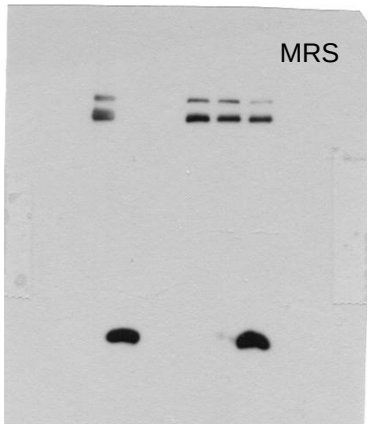

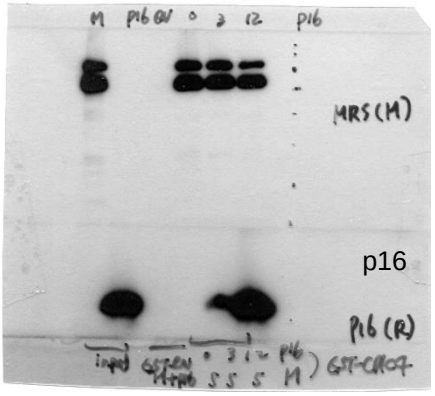

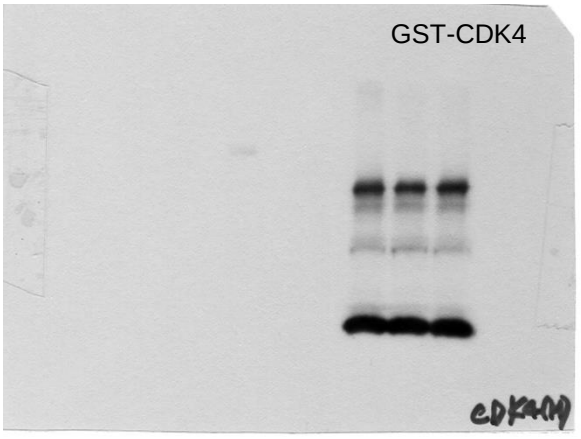

b

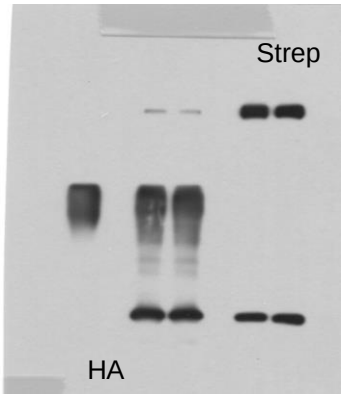

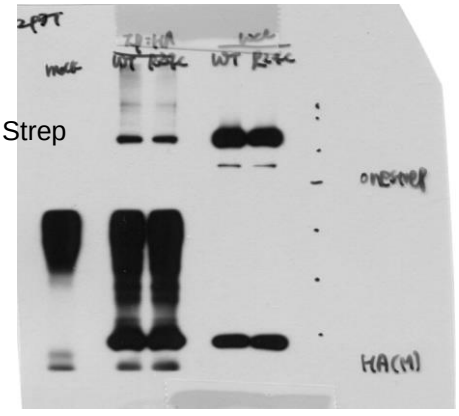

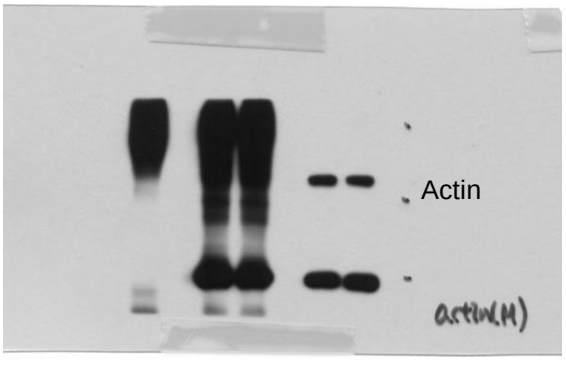

Figure 6. MRS shares interaction site with p16^{INK4a} for the binding to CDK4 but does not disturb the function of CDK4.

C

HA-CDK4 WT transfection / HA-CDK4 R24C transfection

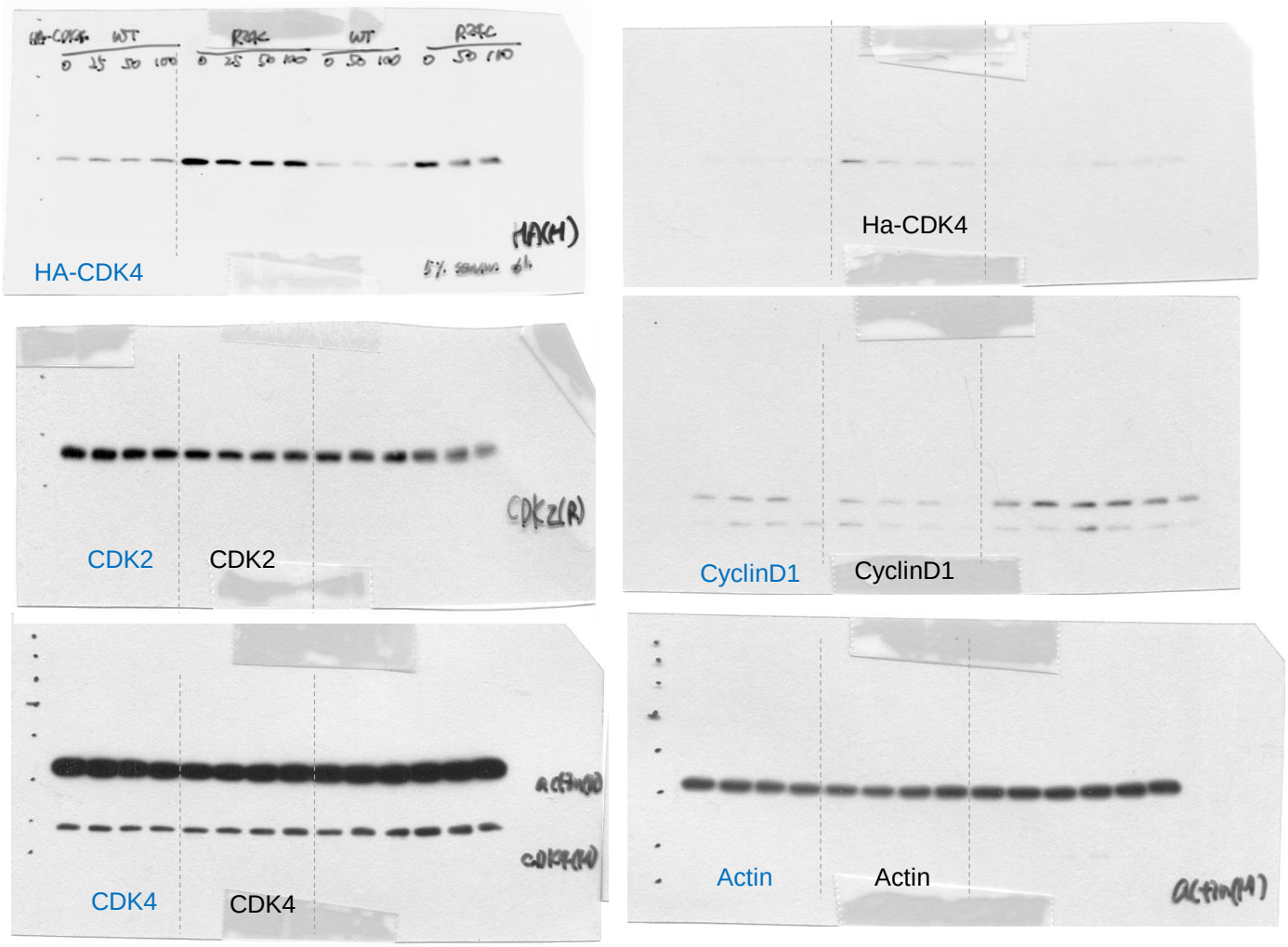

Figure S1. Effect of MRS on global translation in cancer cell lines.

a

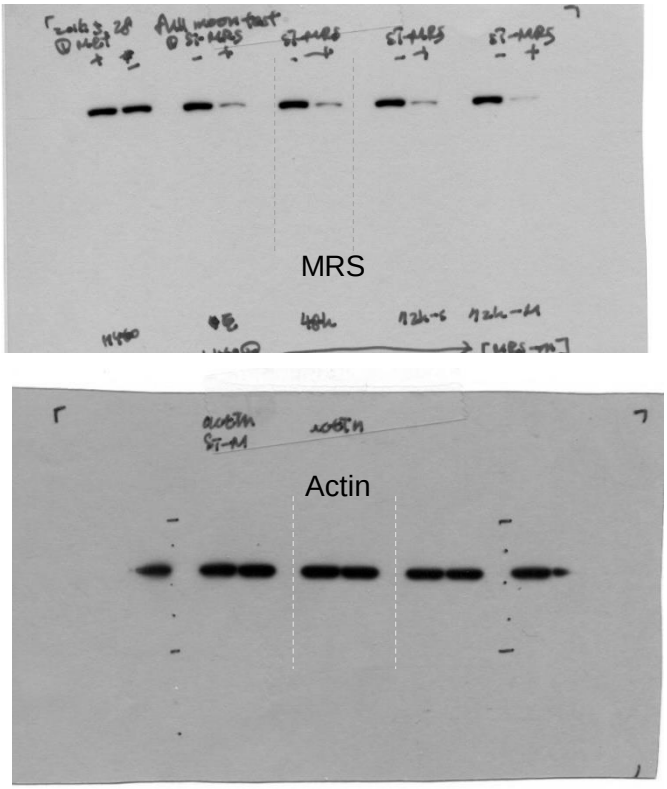

c

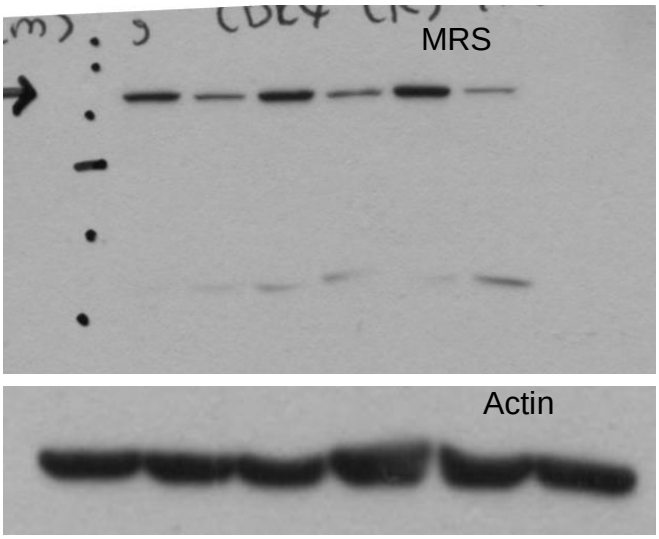

Figure S2 Effect of MRS knockdown on global translation *in vivo*.

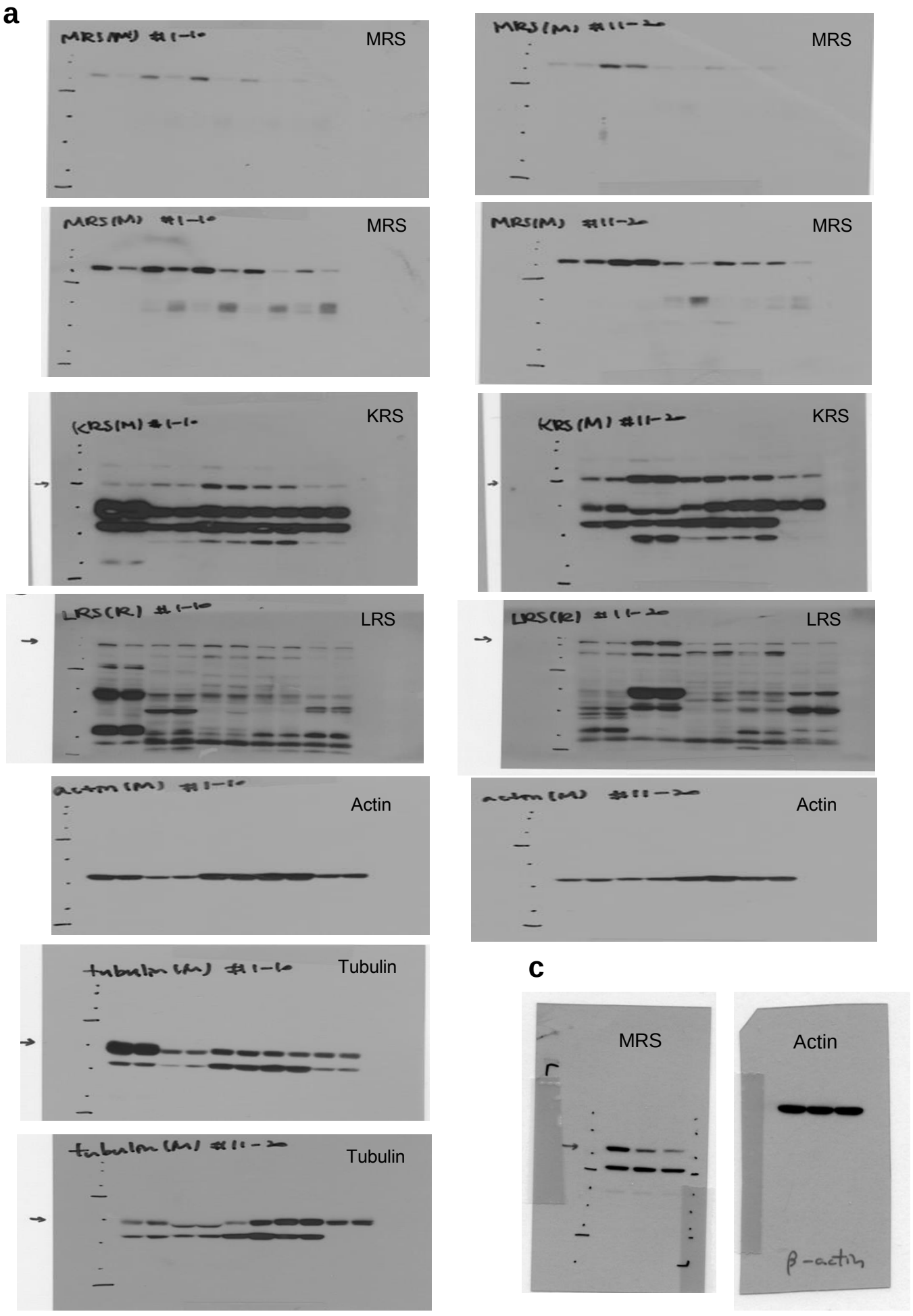

Figure S3 MRS specifically regulates and interacts with CDK4..

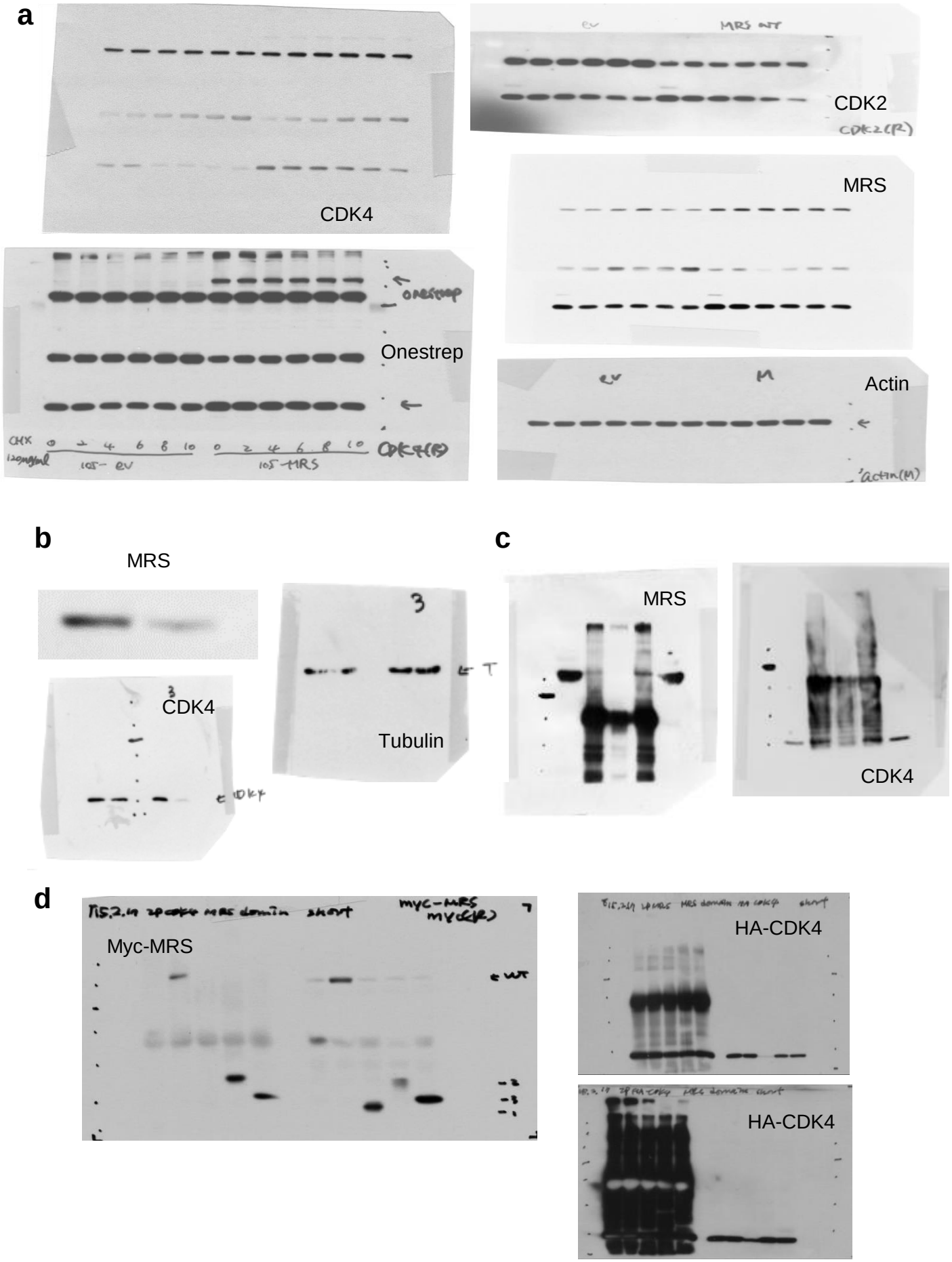

Figure S4 A **s**pecific Met analog FSMO regulates MRS-mediated CDK4 stability mimicking MRS knockdown.

a

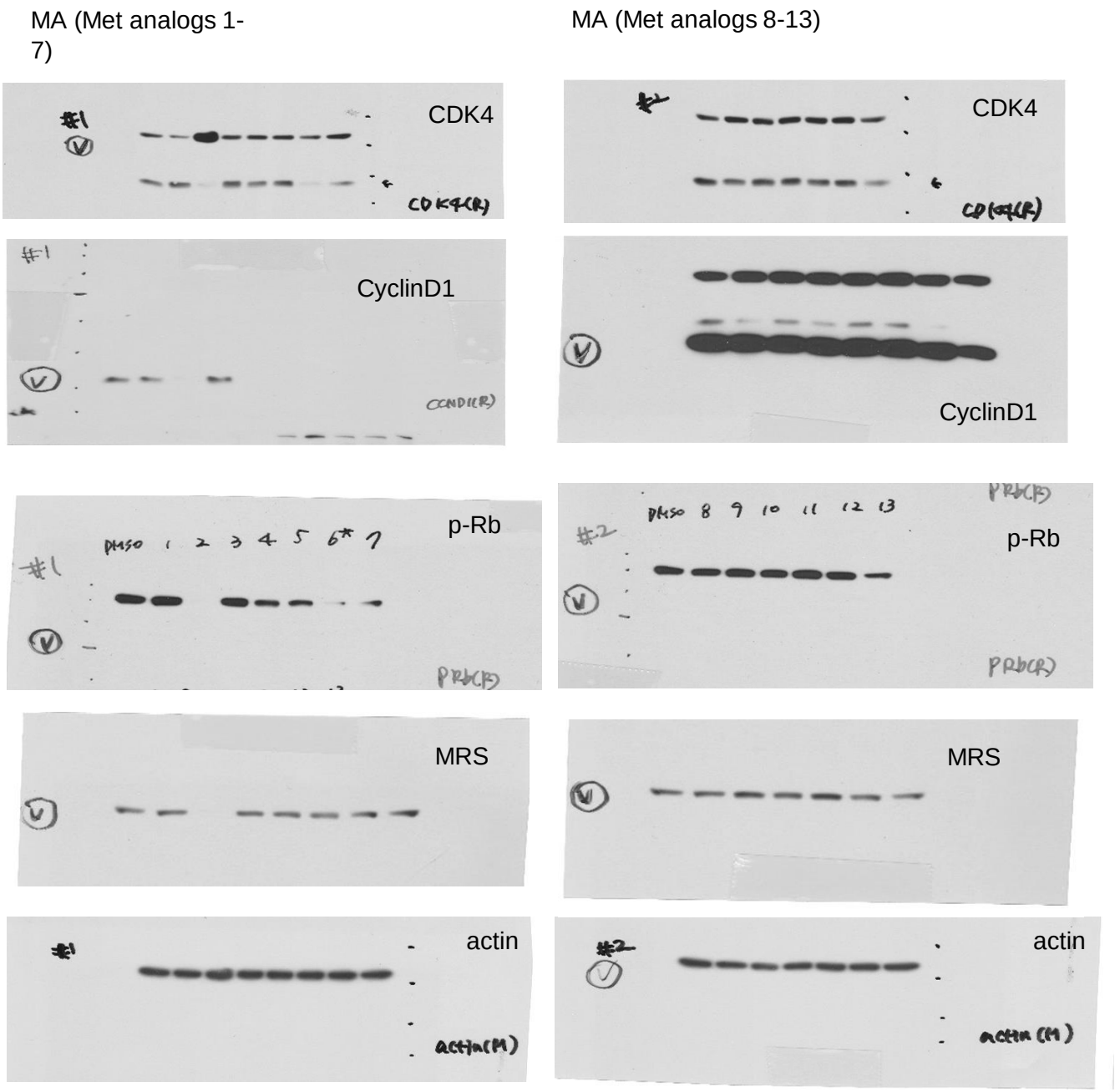

Figure S5 MRS interacts with CDK4 and HSP90.

a

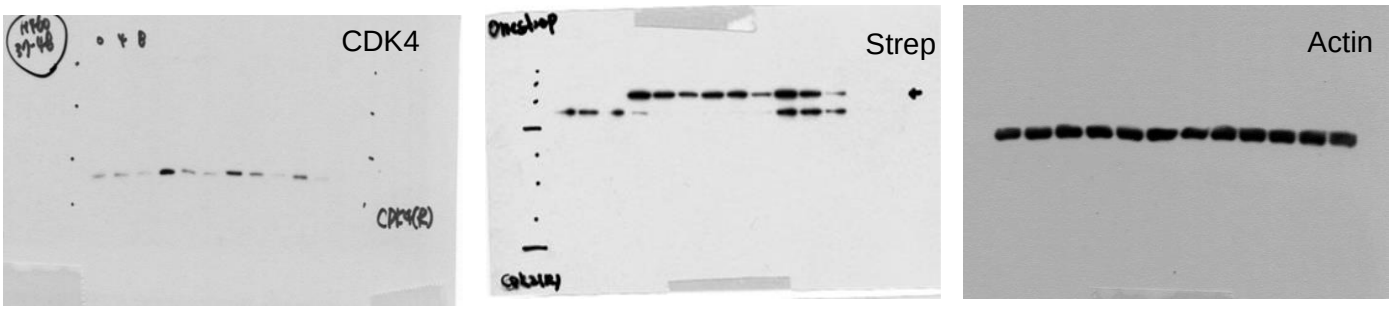

c

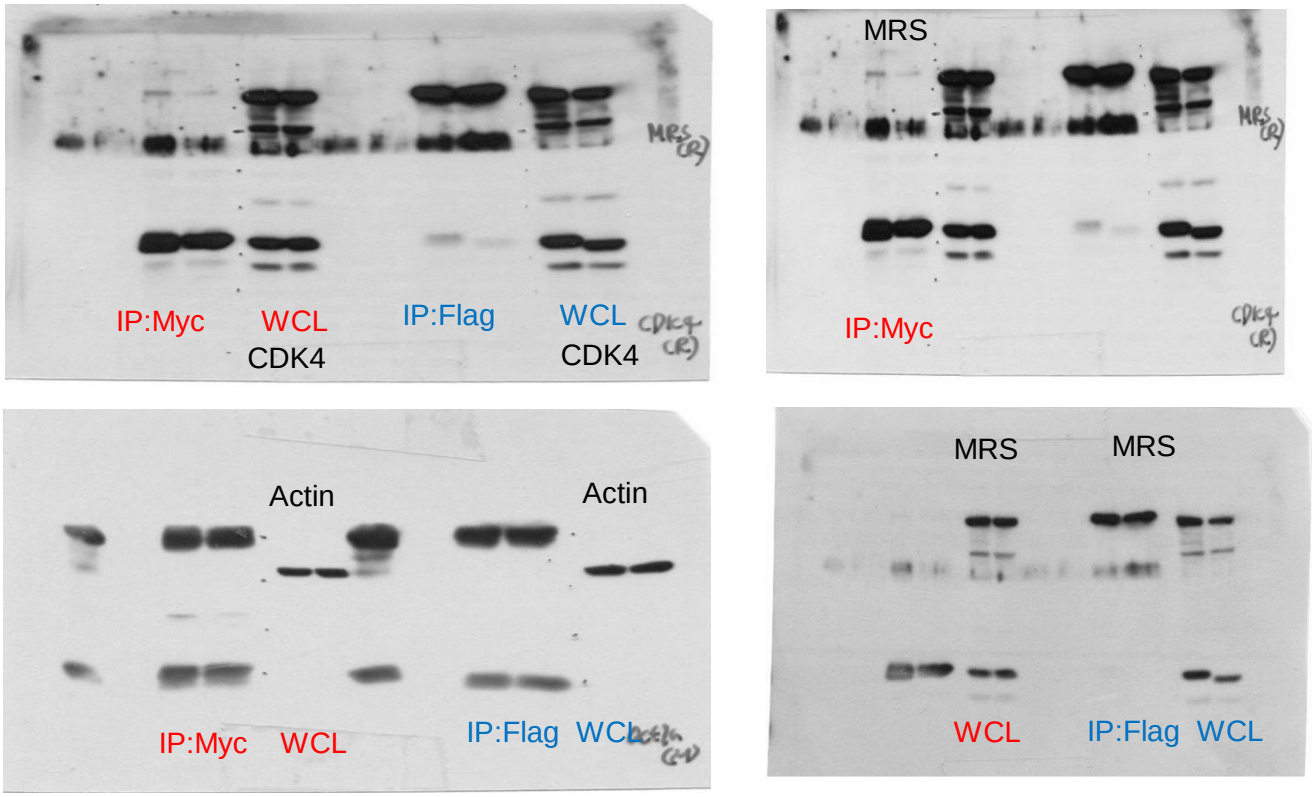

d

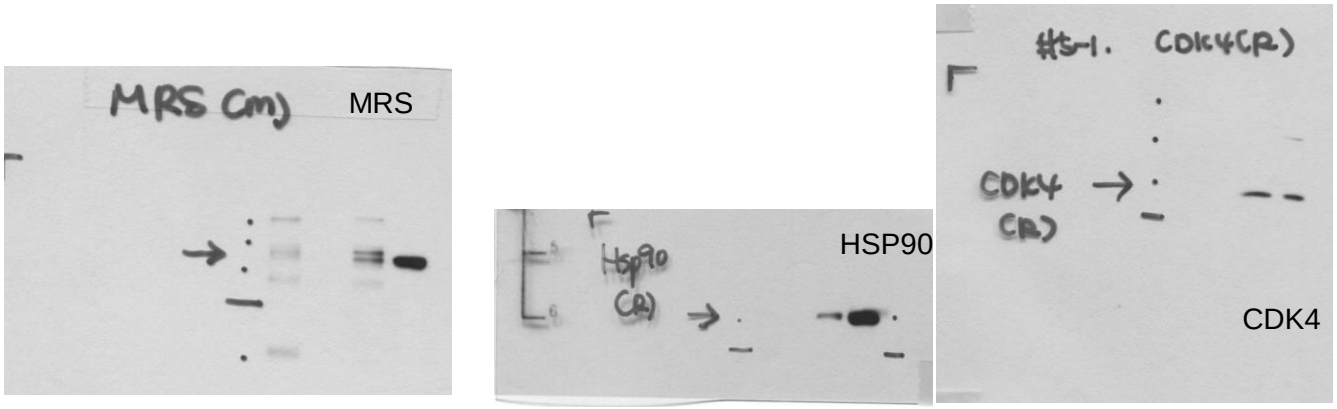

Figure S6 Effect of MRS on CDK4 is dependent to p16^{INK4a} status.

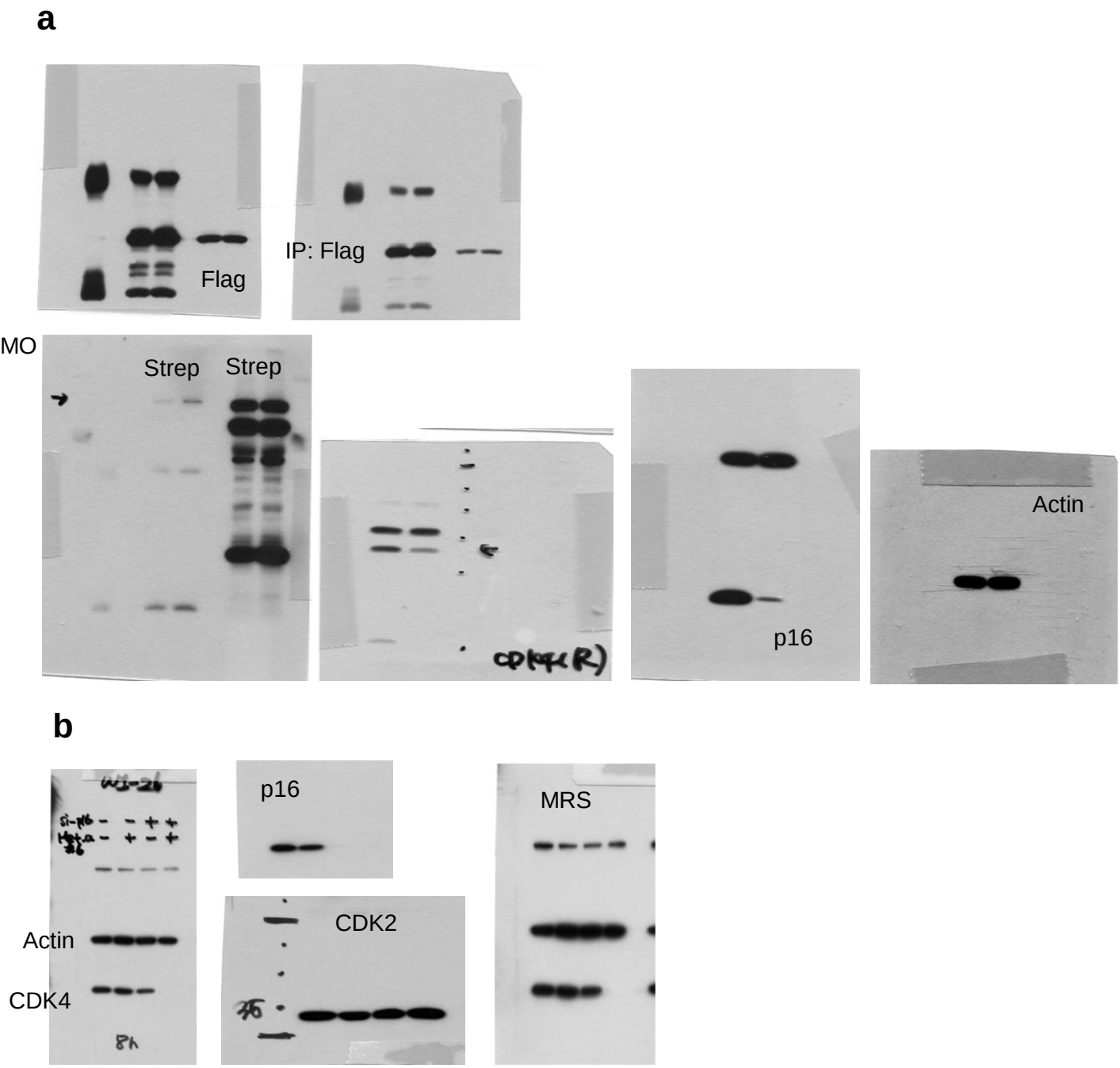

Figure S6 Effect of MRS on CDK4 is dependent to p16^{INK4a} status.

C

293, NIH3T3, WI-26

WI-38, CCD18C0, MCF10A

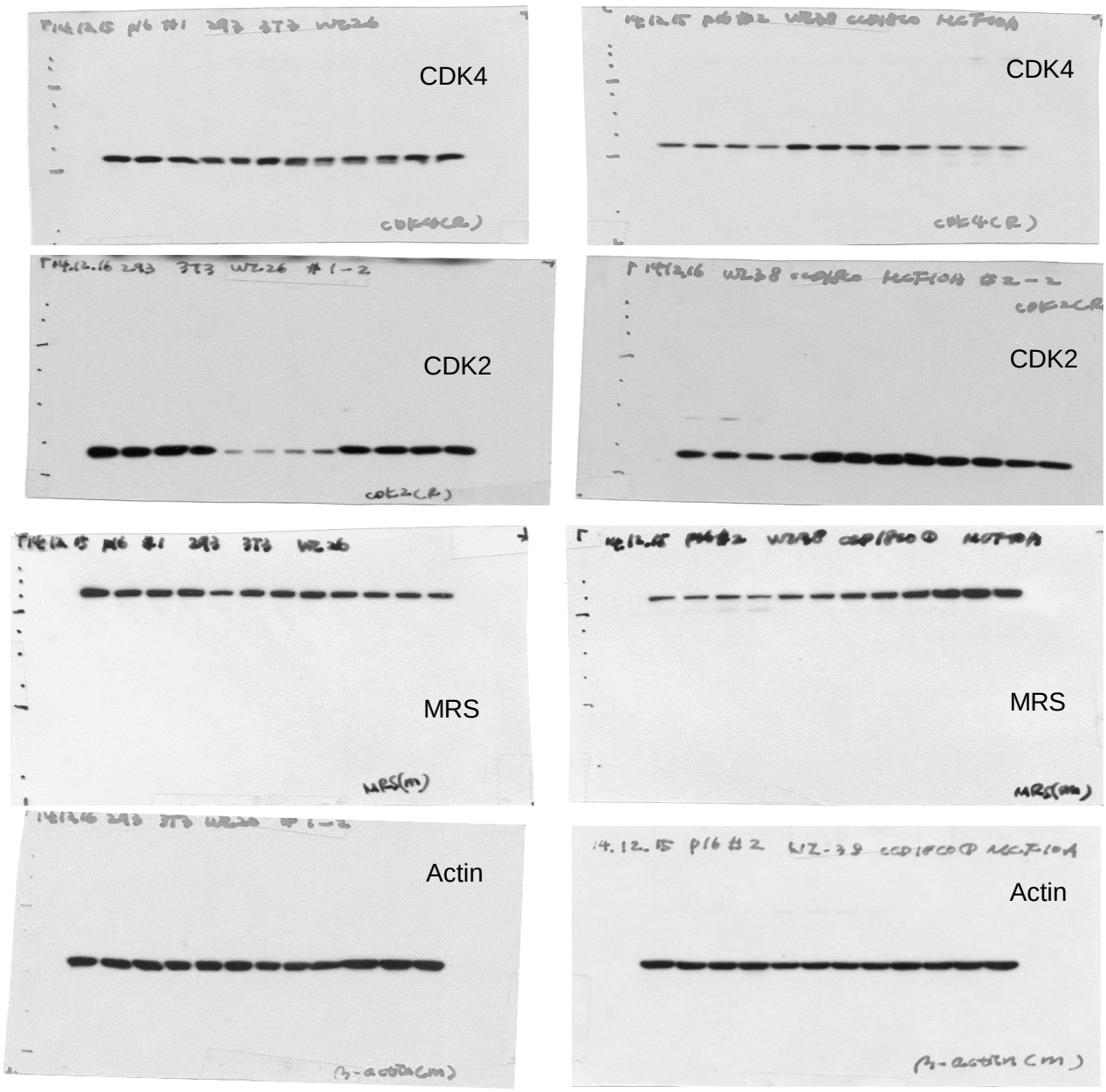

Figure S6 Effect of MRS on CDK4 is dependent to p16^{INK4a} status.

d

HeLa

HCC1937

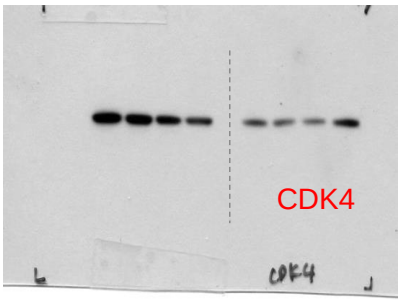

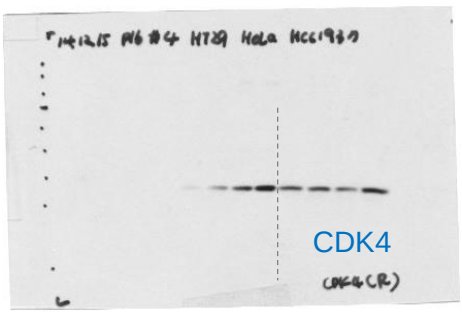

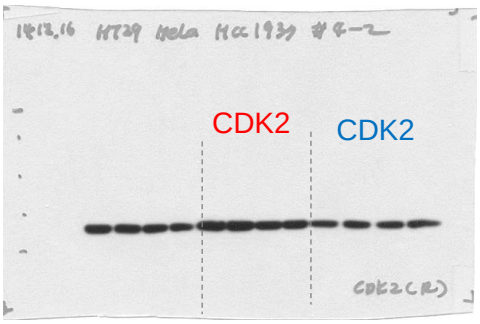

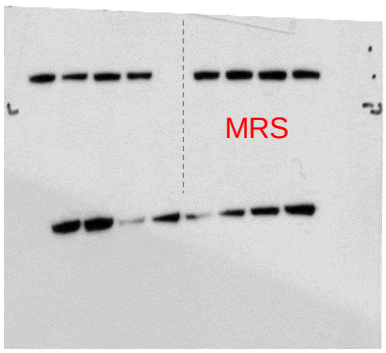

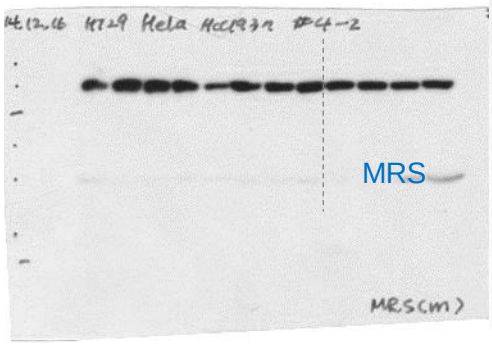

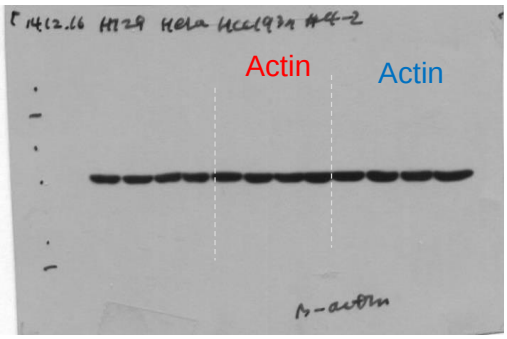

MDA-MB-436, MDA-MB-468

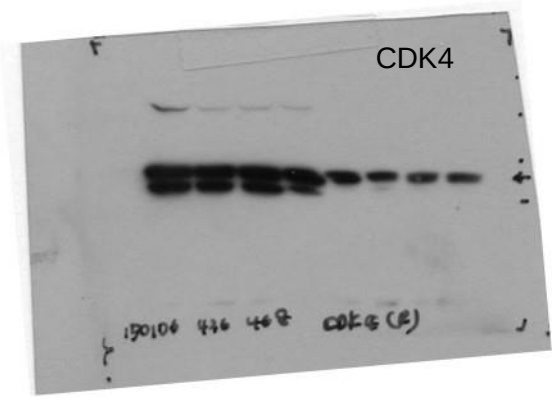

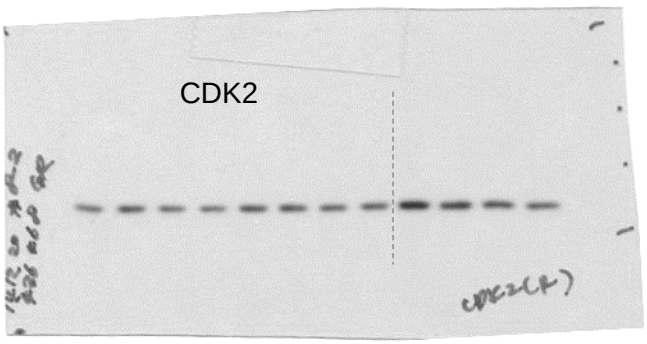

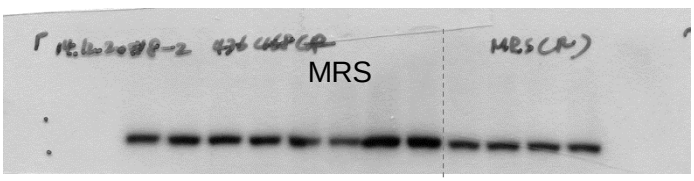

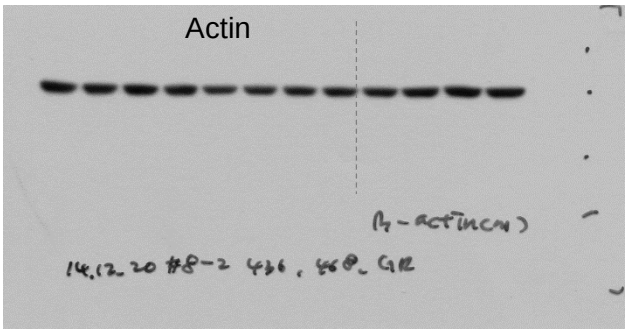

Figure S6 Effect of MRS on CDK4 is dependent to p16^{INK4a} status.

e

A549, H460

MDA-MB-231

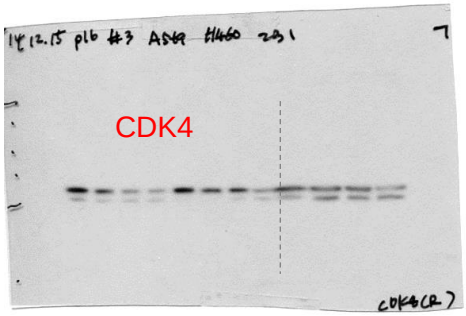

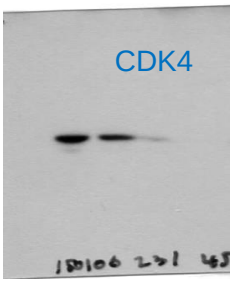

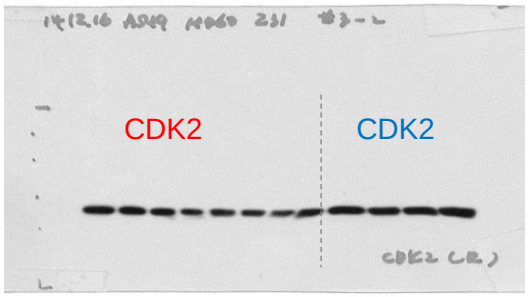

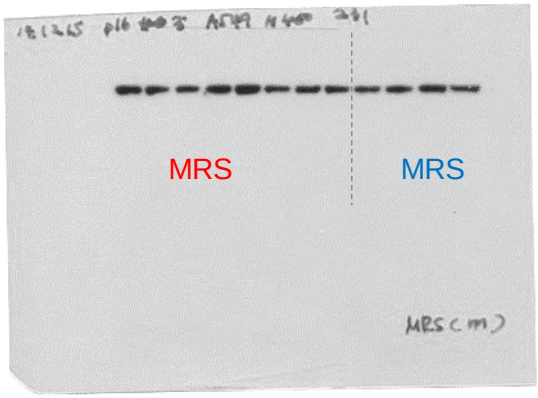

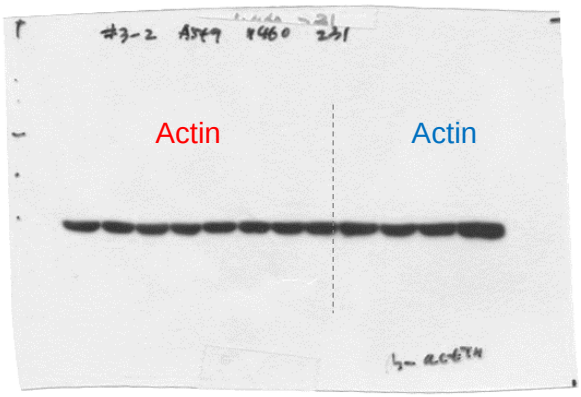

HCT116, H1299, BT20

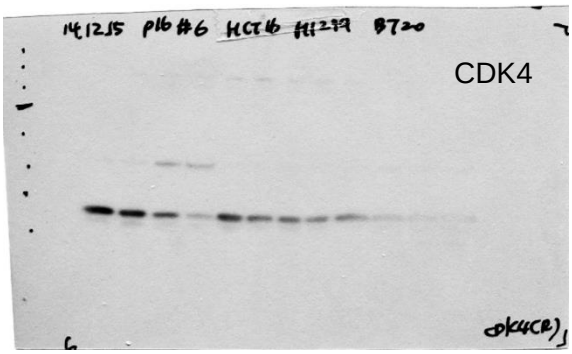

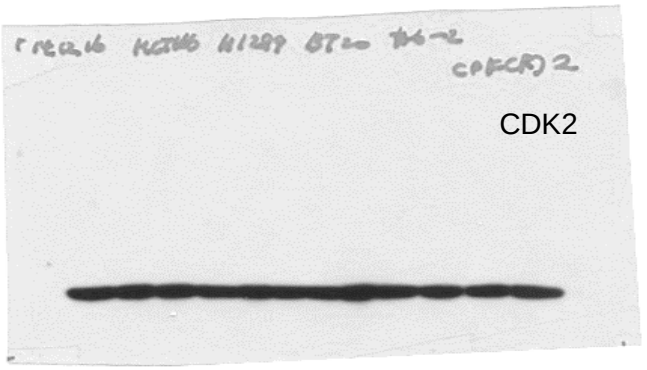

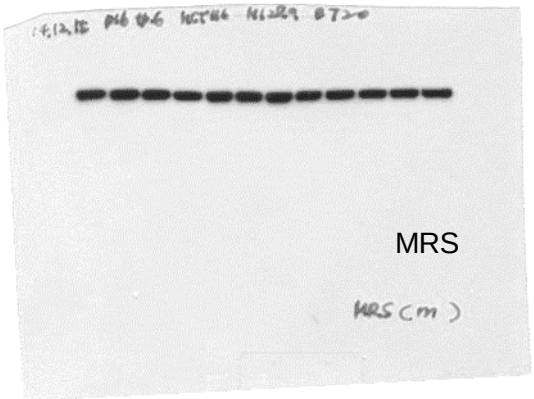

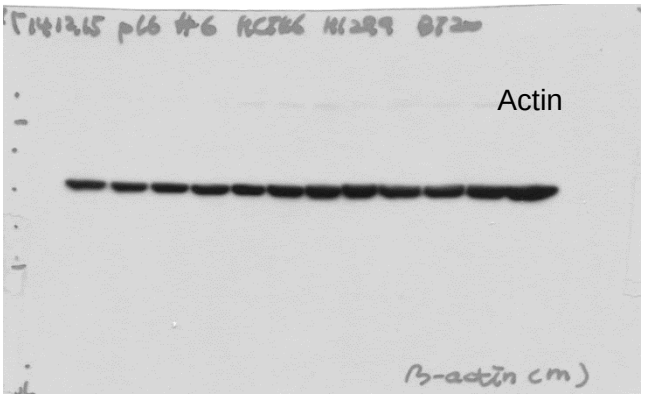

Figure S6 Effect of MRS on CDK4 is dependent to p16^{INK4a} status.